Analysis of plasticity at the supramammillary nucleus to the dentate granule cell synapses

Eri Tabuchi

Graduate School of Brain Science, Doshisha University

A thesis submitted for the degree of
Doctor of Philosophy in Science
March 2024

Abstract

Neurons transmit signals via structures called synapses. Most neurons in the central nervous system have chemical synapses, which convert electrical signals into neurotransmitters to send information. Synaptic transmission changes dynamically in response to the level of neuronal activity, which is called synaptic plasticity. Synaptic plasticity lasts from milliseconds to several days. Especially when it lasts for more than an hour, it is called long-term potentiation (LTP) or long-term depression. Synaptic plasticity is considered to be a basic mechanism for memory and learning.

The dentate gyrus (DG) is the first stage within the hippocampal formation to receive entorhinal cortical inputs and send excitatory outputs to the CA3 region, and plays an important role in memory formation, particularly pattern separation, a process of transforming similar patterns of cortical information to nonoverlapping patterns of CA3 outputs. Through this process, the DG contributes to the encoding and discrimination of memories. The DG also receives subcortical inputs from several brain regions, and these inputs modulate DG functions. Supramammillary nucleus (SuM) is one of the regions projecting to the hippocampus, and this circuit has been implicated in various brain functions. The SuM neurons make monosynaptic connections to granule cells (GCs) and GABAergic interneurons in the DG. These presynaptic boutons co-release the functionally opposing neurotransmitters, glutamate and GABA. Although the SuM-DG pathway

has been implicated in various brain functions, it remains unknown how the SuM afferents to the DG are involved in brain functions at the cellular, synaptic and circuit levels.

In this study, I have examined whether activity-dependent long-term plasticity can be induced at SuM-GC synapses and contributes to DG information processing, to expand the knowledge on the functional roles of the peculiar feature of glutamate/GABA corelease. To measure electrical recordings from acute transverse hippocampal slices from mouse brain, I used electrophysiological techniques and optogenetics. The optogenetic technique made it possible to selectively stimulate nerve fibers projecting from the SuM to the GC among projections from diverse regions. Specific expression of channelrhodopsin-2 at the fibers from SuM to the GCs could be achieved by combining adeno-associated virus and VGluT2-Cre mice. Time resolved, optically induced synaptic responses could be measured by patch-clamp technique.

This study revealed that depolarization of GCs triggered postsynaptic LTP of glutamatergic, but not GABAergic, cotransmission at SuM-GC synapses. Moreover, the burst activity of perforant-path inputs heterosynaptically induced LTP at excitatory SuM-GC synapses. This non-Hebbian LTP required postsynaptic Ca^{2+} influx, Ca^{2+}/calmodulin-dependent protein kinase II activity, and exocytosis of AMPA receptors. Glutamatergic transmission-selective expression of LTP increased the excitatory drive such that SuM inputs alone became sufficient to discharge GCs. Our results highlight a form of LTP, which dynamically and rapidly changes the glutamatergic/GABAergic cotransmission balance and contributes to DG network activity.

Acknowledgement

I would like to thank my supervisor, Dr. Yuki Hashimotodani and Prof. Takeshi Sakaba for their continuous guidance, scientific advice, and encouragement during last 6 years. I would also like to thank Dr. Takafumi Miki and Dr. Ryota Fukaya.

I also extend my feelings of gratitude to Prof. Shigeo Takamori, Prof. Hiroaki Misono and Prof. Susumu Takahashi for being my thesis committee members despite of their busy schedule.

I am grateful to the Doshisha University scholarship for doctoral students and the JSPS predoctoral fellowship for financial support.

Furthermore, I am also profoundly grateful to the past and present members of the Sakaba lab and my friends for their encouragement and good time.

Last but not the least, I would like to thank my family for supporting me.

Table of Contents

Table of Figures

Chapter1. General Introduction

This thesis study focuses on understanding how the synaptic transmission of the supramammillary nucleus to the hippocampus is regulated via synaptic plasticity and in turn regulates the hippocampal circuit, which is important for various brain functions such as learning and memory. Therefore, here I provide introductions to basic mechanisms of synaptic transmission, plasticity, hippocampus circuit, and the supramammillary nucleus.

1.1 Synaptic transmission

Neurons are composed of a lipid bilayer, and due to the restricted permeability of ions, there is an uneven distribution of charges inside and outside the cell. This creates a potential difference known as the membrane potential, typically having a negative value. Ions can move in and out of the cell through ion channels or ion transporters on the cell membrane. When the membrane potential changes in the positive direction, it is called depolarization, and when it changes in the more negative direction, it is called hyperpolarization. If the membrane potential depolarizes beyond a certain threshold, it undergoes a transient and larger depolarization known as an action potential (AP). Neurons are composed of a cell body, dendrites, and an axon, and action potentials originate at the axon hillock, subsequently propagating along the axon to reach the axon terminals. This electrical signal is then transmitted to the next neurons through the specific site

between axons and dendrites called electrical synapses or chemical synapses. In an electrical synapse, the presynaptic and postsynaptic cell membranes are connected directly by special channels called gap junctions. Gap junctions allow ions and small molecules to pass between two neurons, enabling rapid bidirectional electrical signal transmission.

In contrast, chemical synapses convert electrical signals from presynaptic cells into the release of chemical messengers called neurotransmitters. At the presynaptic terminals, neurotransmitters are stored in round intracellular organelles with about 40 nm in diameter called synaptic vesicles (SVs). When APs reach presynaptic terminals, voltage-gated Ca^{2+} channels open. The influx of Ca^{2+} causes SV fusion with the presynaptic membrane, releasing neurotransmitters into 20-100 nm gap (synaptic cleft), the space between the pre and postsynaptic cell membranes. Then neurotransmitters diffuse and bind to specific receptors located on the postsynaptic membranes, leading to excitation or inhibition of the postsynaptic cell. When the postsynaptic cell is excited, the current flowing through the postsynaptic cell is called the excitatory postsynaptic current (EPSC) and the change in membrane potential is called the excitatory postsynaptic potential (EPSP). When the postsynaptic cell is inhibited, the current flowing through the postsynaptic cell is called the inhibitory postsynaptic current (IPSC) and the change in membrane potential is called the inhibitory postsynaptic potential (IPSP) (Fig. 1).

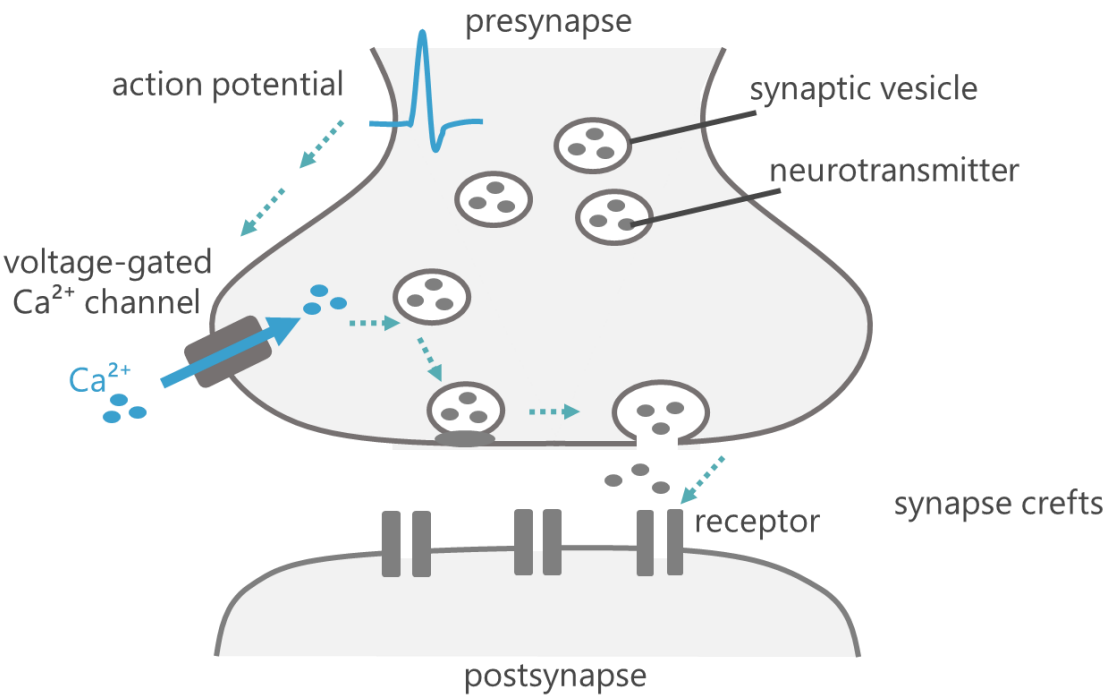

Figure 1. The basic steps of synaptic transmission

Transmission at chemical synapses occurs in the following steps. (a) action potentials arrive at presynaptic terminal. (b) Changes in membrane potential open voltage-gated Ca^{2+} channels. (c) SVs move to the membrane and dock with specific areas on the membrane. Note that it is commonly assumed that this process occurs (mostly) before Ca^{2+} influx, though there is no direct evidence yet. (d) Neurotransmitters are released into the synaptic cleft by exocytosis. (e) Neurotransmitters diffusing into the synaptic cleft bind to receptors on the postsynaptic membrane.

1.2 Neurotransmitter

Neurotransmitters are classified into low molecular weight neurotransmitters and neuropeptides. Low molecular weight neurotransmitters include acetylcholine, biogenic amines, and amino acids. After synthesis in the presynaptic nerve cells, these neurotransmitters are taken up and concentrated into SVs by transporters (Fig. 2). Upon fusion of SVs with the membrane of the presynaptic terminal, neurotransmitters are released into the synaptic cleft. Neurotransmitters not bound to receptors are removed from the synaptic cleft through mechanisms such as diffusion, enzymatic degradation, or reuptake. Acetylcholine and monoamines are reuptaken directly into the synaptic terminal via transporters. In contrast, glutamate and GABA are taken up not only through transporters on presynaptic terminals but also via transporters on glial cells. Neurotransmitters that undergo reuptake into the cell are subsequently reused.

Neuropeptides are synthesized in the cell body and transported to the presynaptic terminal through axonal transport. Unlike low molecular weight neurotransmitters, neuropeptides are stored in secretory vesicles rather than synaptic vesicles. It is known that a single neuron can release both a low molecular weight neurotransmitters and one or more neuropeptides. These neurotransmitters and neuropeptides may either enter different vesicles or coexist in the same vesicle, leading to their simultaneous release. Whether they enter different vesicles or coexist in the same vesicle, this diversity allows for the simultaneous release of these signaling molecules, contributing to the complexity and modulation of neuronal communication at synapses.

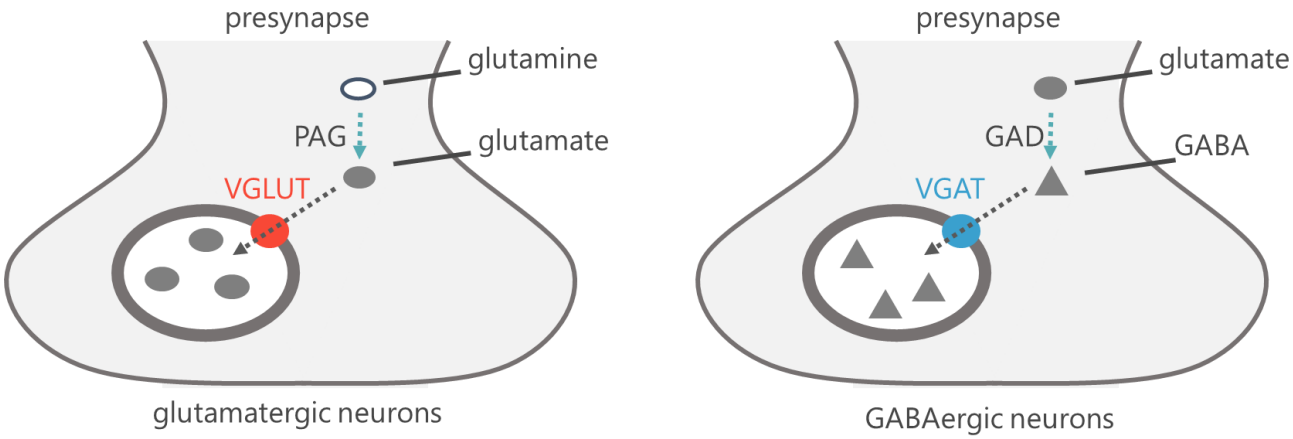

Figure 2. The mechanism of glutamatergic neuron and GABAergic neuron

(Left) Schematic drawing of glutamatergic neuron. Glutamate is synthesized from glutamine by phosphate-activated glutaminase (PAG) in the cytoplasm. Vesicular glutamate transporters (VGLUT) located on the SV membrane are used to transport glutamate into SVs. Mammalian VGLUTs are divided into three subfamilies: VGLUT1, primarily expressed in the cortex and hippocampus; VGLUT2, found in the thalamus, ventromedial hypothalamic nucleus, and amygdala; and VGLUT3, expressed in a limited number of cells. (Right) Schematic drawing of GABAergic neuron. GABA is synthesized from glutamate by glutamic acid decarboxylase (GAD) and enters the SVs via the vesicular GABA transporter (VGAT).

1.3 Neurotransmitter receptors

There are two major types of neurotransmitter receptors: ionotropic and metabotropic receptors. Ionotropic receptors are also called ligand-gated ion channels, and they can be activated by neurotransmitters (ligands). This activation allows specific ions to pass through the membrane, resulting in changes to the postsynaptic membrane potential within a few milliseconds. These ions excite or inhibit postsynaptic cells. In contrast, metabotropic receptors activate intracellular signaling cascades on a scale of tens of milliseconds to seconds. It belongs to the G protein-coupled receptor superfamily and has a broad number of functions such as modulating the conductance of ion channels or triggering a signaling cascade that releases calcium from internal Ca^{2+} stores inside the cell. Most neurotransmitters have both ionotropic receptors and metabotropic receptors.

Neurotransmitter receptors are present on both postsynaptic neurons and presynaptic neurons. Neurotransmitter receptors are known to become unresponsive to the type of neurotransmitter they receive when exposed for extended periods of time.

1.4 Co-releasing neurotransmitters

Classically, it has been believed that one neuron releases only one type of neurotransmitter. However, recent studies have revealed synapses that release multiple neurotransmitters simultaneously. For example, corelease of glutamate and GABA from the same presynaptic terminals in the mature brain has been reported in the lateral habenula from the entopeduncular nucleus (S. J. Shabel et al., 2014; M. L. Wallace et al., 2017; D. H. Root et al., 2018; F. J. Meye et al., 2016) and the ventral tegmental area inputs (D. H. Root et al., 2018; D. H. Root et al., 2014; J. H. Yoo et al., 2016), in the ventral tegmental area from the ventral pallidum inputs (J. H. Yoo et al., 2016), in the CA1 pyramidal cells from subsets of hippocampal interneurons (INs) (K. A. Pelkey et al., 2020; C. Fasano et al., 2017), and from the supramammillary nucleus (SuM) to GCs as shown in this study. In single axon terminals, glutamate and GABA are cotransmitted from distinct synaptic vesicles in the lateral habenula and presumably in the DG (D. H. Root et al., 2018). This peculiar form of synaptic transmission, corelease of neurotransmitters with opposing effects (excitation and inhibition), has led to speculation about several possible synaptic functions, including excitation/inhibition balance, gain control, filtering, and regulation of synaptic plasticity

(N. X. Tritsch et al., 2016; N. Uchida et al., 2014; L. E. Trudeau et al., 2018). Intriguingly, the corelease of glutamate and GABA demonstrates plasticity. In the lateral habenula, GABAergic cotransmission was reduced in animal models of depression (S. J. Shabel et al., 2014) or in the mice of cocaine withdrawal (F. J. Meye et al., 2016). These changes arise from presynaptic modifications, such as impairment of vesicular GABA filling following the reduction of GAD or VGAT. Additionally, in the hippocampal INs, disruption of GABA synthesis by inhibition of GAD or feeding mice a vitamin B6-deficient diet, a manipulation that decreases GAD activity, reduced GABAergic cotransmission with enhanced glutamatergic cotransmission, indicating the homeostatic control of the glutamate/GABA corelease ratio (K. A. Pelkey et al., 2020). Thus, the imbalances in glutamatergic and GABAergic cotransmission are associated with neurological disorders and homeostatic scaling. While these alterations are induced over long time scales (S. J. Shabel et al., 2014; F. J. Meye et al., 2016; K. A. Pelkey et al., 2020), it is unknown whether activity-dependent rapid changes in glutamatergic and GABAergic cotransmission are induced under physiological conditions, and if so, whether such plasticity can modulate overall neural activity in the circuits.

1.5 Synaptic plasticity

Synapses are known to change their strength in an experience-dependent manner, which is called synaptic plasticity. Synaptic transmission can be either enhanced or depressed by activity,

and these changes span temporal domains ranging from milliseconds to hours, days, and presumably even longer. In particular, the plasticity that lasts for more than one hour is called long-term potentiation (LTP) or long-term depression (LTD) (Fig. 3), and these are considered to be elementary processes of learning and memory. There are two major factors that determine the strengths of synaptic transmission: changes in the pre- and post-synapses. Presynaptic factors include the changes in the number of synaptic vesicles available for release and in the probability of synaptic vesicle release. Postsynaptic factors include the changes in the number of neurotransmitter receptors and in their conductance.

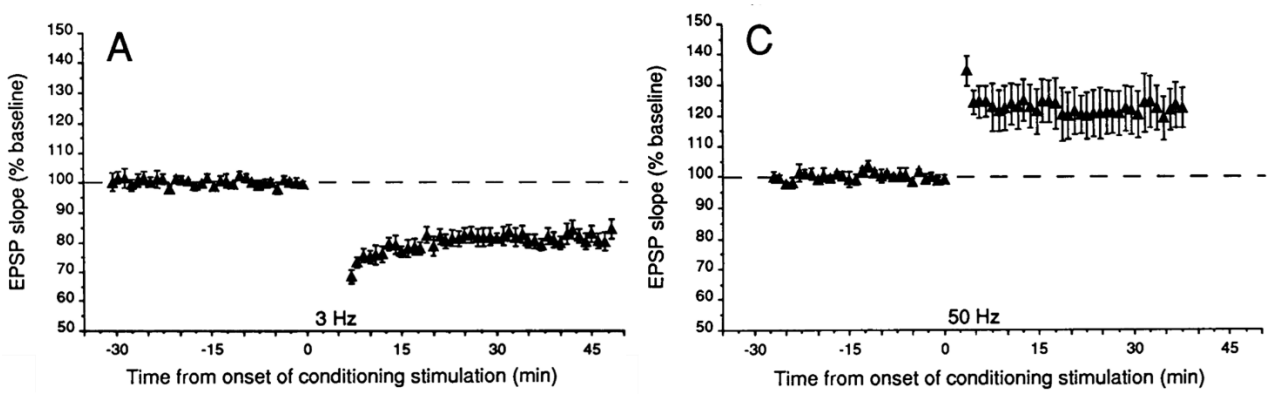

Figure 3. Induction of LTD and LTP by frequent stimulation

Examples of long-term EPSP changes with repetitive stimulation of the Schaffer collateral projection to area CA1 in rat hippocampal slices. (A) 900 pulses at 3 Hz resulted in LTD (81% ± 2% of control at 30 min after conditioning; n=5). (C) 900 pulses at 50 Hz produced potentiation (121% ± 7% of control; n=5). (Dudek SM & Bear MF, 1992, PNAS p4365 Figure 2)

Previous studies have revealed the mechanisms of synaptic plasticity. Among them LTP following the Hebbian rule is considered to be important for elucidating the mechanisms of learning and memory. Hebbian rule means that synaptic connections become stronger when the

presynaptic and postsynaptic parts are activated at the same time. This LTP is N-methyl-D-aspartate receptors (NMDARs) dependent. Ionotropic glutamate receptors have three subtypes: a-amino-3-hydroxy-5-methyl-4-isoxazolepropionic acid receptors (AMPARs), NMDARs, and kainate receptors. AMPARs and kainate receptors share similar properties. AMPARs primarily allow the passage of Na^+ and K^+. On the other hand, NMDARs exhibit unique characteristics. When the membrane potential is negative, the ion channel of NMDARs is blocked by extracellular Mg^{2+}. Depolarization of the postsynaptic membrane removes the Mg^{2+} block. When glutamate is released from the presynaptic terminal and postsynaptic membrane depolarization occur simultaneously, NMDARs predominantly permit the passage of Ca^{2+}. This property, known as a 'coincidence detector', is considered crucial in synaptic plasticity. One of the mechanisms underlying the expression of LTP involves an increase in the number and conductance of AMPARs. AMPARs are present on the membranes of cellular vesicles and on the extracellular membranes outside the synapse. Following the induction of LTP, it has been revealed that receptors on vesicles can be inserted into the postsynaptic membrane through exocytosis, and extracellular receptors can be mobilized. Activation of NMDARs leads to Ca^{2+} influx, activating signaling pathways such as protein kinase A (PKA), protein kinase C (PKC), and Ca^{2+}/calmodulin-dependent protein kinase II (CaMKII). These pathways have been shown to phosphorylate AMPARs, altering conductance and open probability. Additionally, CaMKII is believed to phosphorylate receptor binding proteins and postsynaptic scaffold proteins, contributing to the regulation of synaptic transmission. One

alternative mechanism for LTP involves changes in the presynaptic region. LTP occurring at the mossy fiber-CA3 synapse in the hippocampus does not involve NMDARs. Mainly, LTP occurs by altering the release probability of neurotransmitters through cyclic adenosine monophosphate (cAMP) and PKA signaling.

1.6 Hippocampus

The hippocampus, which is located in the inner region of the temporal lobe, forms part of the limbic system, which is particularly important in regulating emotional responses. It is thought to be involved in an important role in learning and memory formation. The hippocampus is composed of several subregions, including the cornu ammonis (CA1-3), the dentate gyrus (DG), and the subiculum. The major cells in each region are granule cells (GCs) in the DG and pyramidal cells in CA1-CA3. Santiago Ramon y Cajal found the major neural circuit in the hippocampus. The cortex transmits information to the hippocampus via the entorhinal cortex (EC). This signal is sent to the GCs in the DG via the perforant-path. Then, the GCs transmit signals to pyramidal cells in CA3 via mossy fibers. Pyramidal cells in CA3 send signals to pyramidal cells in CA1 via Schaffer collaterals. Finally, pyramidal cells in CA1 transmit signals to the EC (Fig. 4). This circuit, composed of these three cell-types, is called the trisynaptic circuit, and the functional roles of the circuit has been studied by many researchers. In contrast to the trisynaptic circuit, the inputs driving the GCs has been studied only recently.

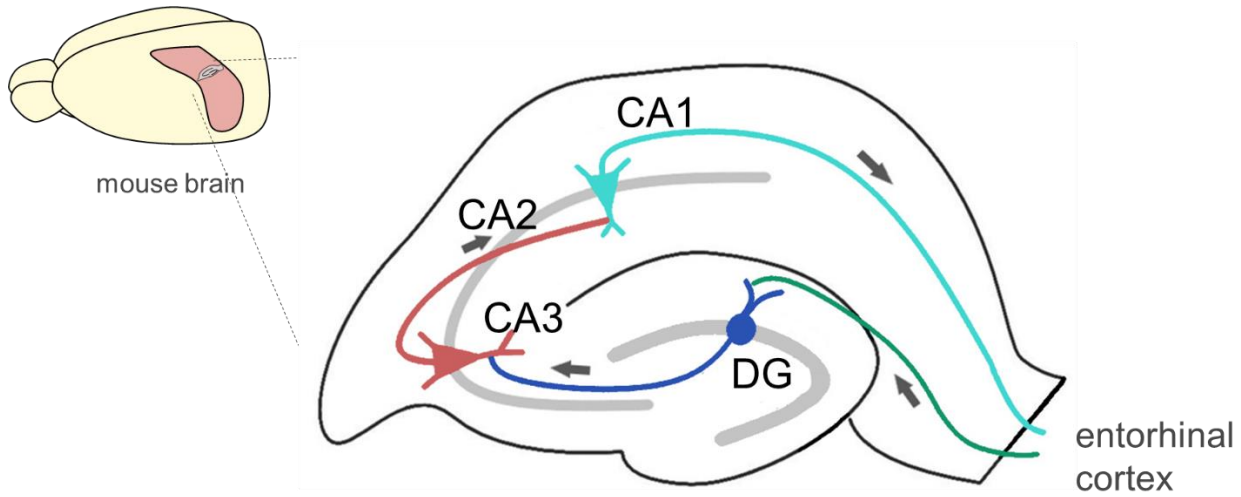

Figure 4. Trisynaptic circuit in hippocampus

Schematic drawing of hippocampal slice. Signals from the entorhinal cortex are sent to the GCs in the DG, which send the signal through mossy fibers to the pyramidal cells in CA3. From CA3, the signals are sent further to CA1.

1.7 Supramammillary nucleus

The supramammillary nucleus (SuM) of the hypothalamus is one subcortical region that projects to the DG and CA2 region (L. Haglund et al., 1984; R. P. Vertes, 1992). SuM can be divided into medial and lateral parts. Medial SuM has small dopaminergic cells, which project to the lateral septal nucleus, not to the hippocampus. Lateral SuM has large cells which project to the hippocampus (W. X. Pan & N. McNaughton, 2004). With direct connections and indirect connections via the medial septum to the hippocampus, SuM activity is involved in the hippocampal θ rhythm (W. X. Pan & N. McNaughton, 2004; R. P. Vertes & B. Kocsis, 1997). Recent studies have indicated that the SuM projection to the DG is related to spatial memory retrieval (Y. Li et al., 2020), sleep and arousal (N. P. Pedersen et al., 2017; L. Renouard et al., 2015; F. Billwiller et al., 2020), and contextual novelty (S. Chen et al., 2020). Interestingly,

Hashimotodani et al. (2018) have shown that SuM inputs to DG are mediated by co-release of glutamate and GABA. However, whether glutamate and GABA are co-packed in the same SVs or segregated into distinct vesicle population at the same presynaptic terminals has not been firmly established.

1.8 Research aims

The aim of this research is to examine whether activity-dependent long-term plasticity can be induced at SuM-GC synapses and contributes to DG information processing. Recent studies have revealed that the SuM neurons make monosynaptic connections to GCs, the DG principal neurons, and corelease glutamate and GABA on to GCs (N. P. Pedersen et al., 2017; F. Billwiller et al., 2020; S. Chen et al., 2020; Y. Hashimotodani et al., 2018; M. I. Ajibola et al., 2021). This glutamatergic and GABAergic cotransmission exerts a net excitatory effect on GCs and modulates GC firing through temporal association with entorhinal cortical inputs (Y. Hashimotodani et al., 2018; M. I. Ajibola et al., 2021). Despite emerging evidence that the SuM-DG pathway contributes to several brain functions, it remains unknown how the SuM afferents to the DG are involved in brain functions at the cellular, synaptic and circuit levels.

In this study, I first examined whether the synaptic transmission between SuM and GCs exhibits activity-dependent long-term plasticity. I found that repetitive depolarizing pulses on to the GCs or burst firing of MPP induced glutamatergic cotransmission-selective LTP at SuM-GC synapses. The SuM-GC LTP is expressed postsynaptically and requires Ca^{2+} influx through L-type

voltage-dependent Ca^{2+} channels (L-VDCCs), postsynaptic CaMKII activity, and possibly exocytosis of AMPAR. By selective expression of glutamatergic— but not GABAergic—LTP, glutamatergic transmission plays a dominant role in SuM-GC synaptic transmission and excites GCs to trigger action potentials (APs). Thus, these findings provide evidence that SuM-GC glutamate/GABA corelease synapses undergo rapid and enduring activity-dependent changes in synaptic transmission, and such synaptic plasticity may modulate DG information processing and contribute to SuM-DG circuit-linked brain functions.

Part of the thesis has been published in Eri Tabuchi et al. (2022) "Excitatory selective LTP of supramammillary glutamatergic/GABAergic cotransmission potentiates dentate granule cell firing", volume119, e2119636119, PNAS (Copyright (2022) National Academy of Science)

Chapter2. Material and Methods

2.1 Animals

I used C57BL/6 mice, VGluT2-Cre mice (Jackson labs, Slc17a6$^{tm2(cre)Lowl}$/J, stock #016963) and VGAT-Venus mice (D. G. Amaral et al., 2007) crossed with VGluT2-Cre mice (VGluT2-Cre/VGAT-Venus) of either sex for electrophysiological experiments. All animals were group housed in a temperature- and humidity-controlled room under a 12 hr light/12 hr dark cycle. Water and food were available *ad libitum*. Experiments were approved by the animal care and use committee of Doshisha University, and were performed in accordance with the guidelines of the committees.

2.2 Stereotaxic viral injections

Mice of postnatal days 19 to 20 were placed in a stereotaxic frame, and anesthetized with isoflurane (1.5-2.5%). A beveled glass capillary pipette connected to a microsyringe pump (UMP3, WPI) was used for viral injection. 200 nL of a virus-containing solution was injected into the SuM (relative to bregma, AP: –2.2 mm, ML: ±0.3 mm, DV: –4.85 mm) at a rate of 50 nL/min. The glass capillary was remained at the target site for 5 min before the beginning of the injection and was removed 10 min after infusion. VGluT2-Cre mice and VGluT2-Cre/VGAT-Venus mice were injected with adeno-associated virus (AAV); AAV1.EF1a.DIO.hChR2(H134R)-eYFP (Addgene) or AAV1.EF1a.DIO.hChR2(H134R)-mCherry (Addgene), respectively (Fig. 5).

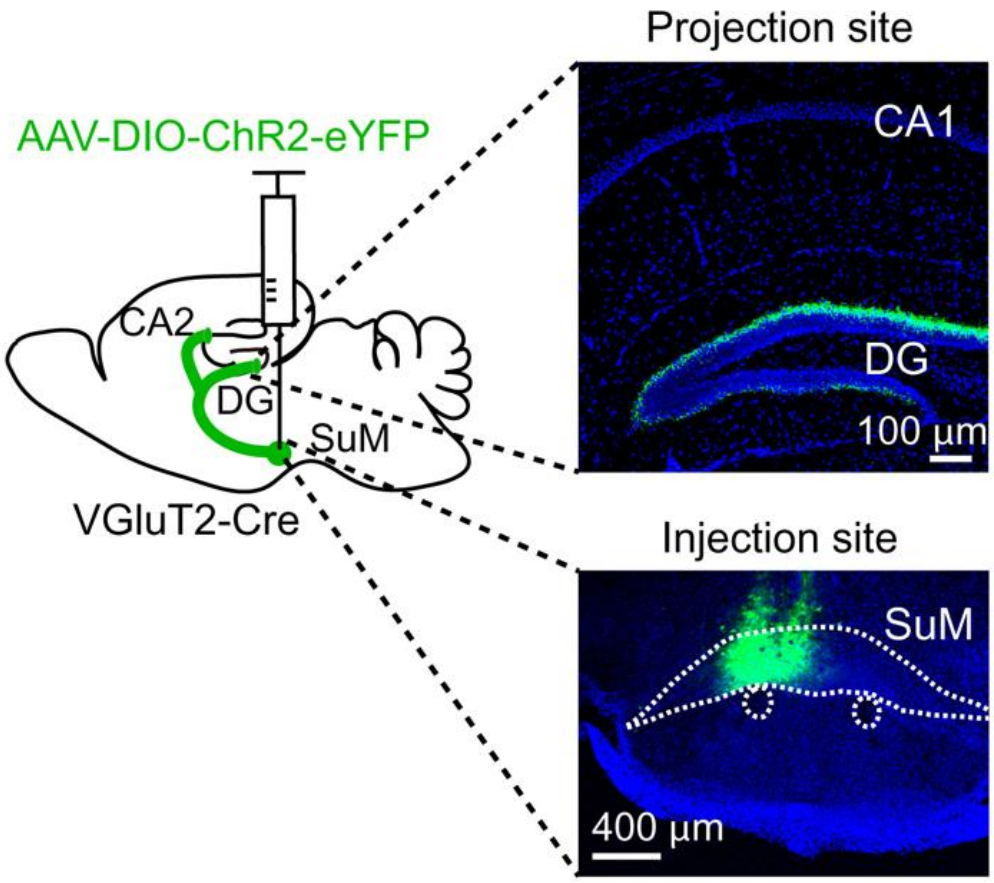

Figure 5. The site of AAV injection

(Left) Diagram illustrating injection of AAV-DIO-ChR2(H134R)-eYFP into the SuM of VGluT2-Cre mouse. (Right) Confocal images showing ChR2(H134R)-eYFP-expressing SuM axons in the DG (Upper) and injection site (Lower).

2.3 Hippocampal slice preparation

Acute transverse hippocampal slices (300 μm thick) were prepared from mice 2-3 weeks after the injection of AAVs (5-6 weeks old). Mice were decapitated under isoflurane anesthesia. Briefly, the hippocampi were isolated, embedded in an agar block and cut using a vibratome (VT1200S, Leica microsystems) in an ice-cold cutting solution containing (in mM): 215 sucrose, 20 D-glucose, 2.5 KCl, 26 $NaHCO_3$, 1.6 NaH_2PO_4, 1 $CaCl_2$, 4 $MgCl_2$, and 4 $MgSO_4$. Brain blocks including the interbrain and midbrain were also isolated and fixed in 4% paraformaldehyde (PFA)

for *post hoc* morphological analysis of the injection site. Hippocampal slices were transferred to an incubation chamber and incubated at 33.5°C in the cutting solution. After 30 min of incubation, the cutting solution was switched to an extracellular artificial cerebrospinal fluid (ACSF) containing (in mM): 124 NaCl, 2.5 KCl, 26 $NaHCO_3$, 1 NaH_2PO_4, 2.5 $CaCl_2$, 1.3 $MgSO_4$ and 10 D-glucose at 33.5°C. Slices were subsequently kept at room temperature for at least 1 h before recording. Both the cutting solution and ACSF were oxygenated with 95% O_2 and 5% CO_2. After the recovery time, slices were transferred to a submersiontype recording chamber and perfused at 2 mL/min with oxygenated ACSF.

2.4 Electrophysiology

Whole-cell recordings were made from GCs, INs, and CA2 pyramidal neurons under an infrared differential interference contrast microscopy (IR-DIC, Olympus, BX51WI). For voltage-clamp recordings (V_{hold} = –60 mV), I used patch pipettes (3-6 MΩ) filled with an intracellular solution containing (in mM): 110 Cs-gluconate, 17.5 CsCl, 0.2 EGTA, 10 HEPES, 8 NaCl, 2 MgATP, 0.3 Na_3GTP, 10 phosphocreatine, pH 7.3 adjusted with CsOH (290-293 mOsm). For recordings of IPSCs, CsCl was increased to 53 mM, and equimolar amount of Cs-gluconate was removed (calculated E_{Cl^-} = –20 mV). I recorded from GCs with an input resistance of < 300 MΩ for mature GCs (J. J. Knierim & J. P. Neunuebel, 2016). For recordings from INs in the DG, I used VGAT-Venus BAC transgenic mice, in which Venus fluorescent proteins are expressed under the

control of the VGAT promotor, enabling us to identify VGAT-expressing GABAergic neurons (D. G. Amaral et al., 2007). VGAT-Venus mice were crossed with VGluT2-Cre mice for Cre-dependent expression of ChR2. INs were visually identified as Venus-expressing cells located at the border between the GC layer and the hilus, as reported previously (T. D. Goode et al., 2020). For recordings from CA2 pyramidal neurons, 0.5% biocytin was included in the intracellular solution for *post hoc* morphological analysis. CA2 pyramidal neurons were identified based on the location, size of the soma, and electrophysiological properties (firing properties and sag amplitude) (T. Hainmueller & M. Bartos, 2020; L. Haglund et al., 1984). ChR2-expressing SuM axons were activated at 0.05 Hz by a pulse of 470 nm blue light (5 ms duration, 10.5 mW/mm^2) delivered through a 40 x objective attached to a microscope using an LED (Mightex or ThorLabs). The blue light pulses induce inward currents, optically evoked excitatory postsynaptic currents (oEPSCs). For extracellular fiber stimulation, a patch pipette with a broken tip (with diameter of ~20-30 μm) filled with the ACSF was used. Depol-eLTP was typically induced by repeated postsynaptic depolarizations (2 s duration repeated 10 times every 5 s from a holding potential of –60 mV to 0 mV). This depol-eLTP protocol was delivered within 20 min after whole-cell break-in. The pairing protocol was applied by 200 light pulses at 2 Hz paired with 100 s duration postsynaptic depolarization from –60 mV to 0 mV. For recordings of asynchronous synaptic events in the presence of strontium, ACSF was replaced by Ca^{2+}-free ACSF containing 8 mM $SrCl_2$. Asynchronous synaptic responses were evoked by light pulses at 0.1 Hz. After obtaining 10 min

baseline, extracellular solution was replaced by normal ACSF containing 2.5 mM Ca^{2+} to deliver the depol-eLTP protocol, and then extracellular solution was returned to Sr^{2+}-containing ACSF. To test the effects of postsynaptic depolarization on NMDAR-oEPSCs, baseline responses were recorded with stimulus intensities yielding 30-50% of the maximum response to avoid putative saturation of NMDAR activation during the baseline period. For recordings of silent synapses, after obtaining oEPSCs at –60 mV, the light intensity was reduced to the point where a decrease in the rise time of oEPSCs was clearly distinguished (1 ms duration, 0.2-2.0 mW/mm^2) (20-80% rise time: before; 1.14 ± 0.22 ms, after; 2.99 ± 0.31 ms, n = 9, $p < 0.01$, paired t test). Only cells having a constant recording of oEPSCs with a slow rise time (NMDAR-oEPSCs) during baseline were used for the experiments. Series resistance (8-18 MΩ) was uncompensated and monitored throughout experiments with a –5 mV, 50 ms voltage step, and cells that exhibited a significant change in the series resistance more than 20% were excluded from analysis.

For current-clamp recordings, I used an intracellular solution with the following composition (in mM): 136 K-gluconate, 4 KCl, 10 HEPES, 0.2 EGTA, 5 NaCl, 2 MgATP, 0.3 Na_3GTP, 10 phosphocreatine, pH 7.3 adjusted with KOH (288-294 mOsm). In Fig. 7C, 20 mM K-gluconate was replaced with 20 mM BAPTA. Input resistance was monitored throughout the experiments with a hyperpolarizing current injection (200 ms, 20 pA), and data were excluded if the input resistance changed by more than 30%. Burst-firing-induced LTP was induced in current-clamp mode by theta frequency current injection (10 bursts of 40 ms current injection, which

elicited 3-4 APs, at 5 Hz, repeated 5 times every 5 s). For TBS, the stimulation electrode was placed in the middle molecular layer to activate the MPP, and TBS was induced by a series of 10 bursts of 5 stimuli (100 Hz within the burst, 200 ms interburst interval) delivered five times every 10 s.

Recordings were performed using an EPC10 (HEKA Electronik) or IPA amplifier (Sutter Instruments). Data were filtered at 2.9 kHz and sampled at 20 kHz. Liquid junction potentials were not corrected, unless otherwise stated. Bath solutions contained picrotoxin (100 μM) for recordings of EPSC(P)s, and NBQX (10 μM) and D-AP5 (50 μM) for recordings of IPSCs, unless otherwise stated.. All experiments were performed at 28 ± 1°C, except for Fig. 7C, 13H, 15, 16, 17 where experiments were performed at near physiological temperature (31-34°C). Temperature was controlled using a temperature controller (TC-324C, Warner Instruments).

2.5 Pharmacology

Each reagent of stock solution was dissolved in water or DMSO, depending on the manufacture's recommendation and stored at –20°C. NBQX, D-AP5, DCG-IV, LY341495, and AM251 were purchased from Tocris Bioscience. AIP, Gö6983, CPA, and H89 were purchased from Cayman Chemical. BoTx was purchased from R&D systems. KN-93 and picrotoxin were purchased from Tokyo Chemical Industry. Nifedipine was purchased from Nacalai tesque. NEM was purchased from FUJIFILM Wako Chemicals. BAPTA was purchased from Dojindo Laboratories. Reagents were bath applied following dilution into ACSF from stock solutions just before use. For

experiments requiring postsynaptic loading reagents, the LTP induction protocol was applied at least 15-20 min after establishing whole-cell configuration. CPA, H89, Gö6983, and KN-93 were preincubated with slices for at least 1 h and were always included in the bath solution. Control and test conditions were interleaved for all experiments.

2.6 Histology and fluorescence imaging

For *post hoc* confirmation of the injection site, SuM-containing brain blocks obtained in the preparation of hippocampal slices were kept overnight in 4% PFA and then washed in PBS. Tissues were embedded in 1.5% low-melting-point agarose and sagittally sectioned at 100 μm using a vibratome (DTK-1000N, Dosaka). Fluorescence images were acquired using a fluorescence microscope (BZ-X800, Keyence).

To study the expression of ChR2(H134R)-eYFP, ChR2(H134R)-mCherry, and Venus, AAV-injected mice under deep pentobarbital anesthesia (100 mg/kg of body weight, intraperitoneally) were perfused with 4% PFA. Brains were removed and stored in 4% PFA for 4 h at room temperature, then transferred to PBS and left overnight at 4°C. Coronal brain slices containing the SuM or the hippocampus were sectioned at 100 μm using a vibratome (DTK-1000N, Dosaka). Sections were rinsed twice in PBS and mounted on glass slides with DAPI. For *post hoc* morphological analysis of the recorded neurons, slices were fixed in 4% PFA overnight at 4°C. Slices were then washed with PBS and incubated with streptavidin-conjugated Alexa Fluor 568

(1:500, Thermo Fisher Scientific) in PBS and 0.1% Triton X-100 overnight at room temperature. After washing 5 times with PBS, the slices were mounted on glass slides with DAPI. Fluorescence images were acquired using a confocal microscope (TCS SP8, Leica microsystems) and analyzed using the ImageJ (NIH).

2.7 Data analysis

The magnitude of LTP was determined by comparing 10 min baseline responses (or 5 min in Fig. 6, 15) with the last 10 min responses after LTP induction shown in each experiment. PPR was defined as the ratio of the amplitude of the second EPSC to the amplitude of the first EPSC (100 ms interstimulus interval). PPR was measured 10 min before and 30-40 min (or 0-5 min for Fig. 10) after LTP induction. The asynchronous events were measured during a 700 ms period beginning 30 ms after light stimulus in order to exclude the initial synchronous synaptic responses. The amplitude and frequency of the asynchronous events were compared before (10 min baseline) and after (20 min after depol-eLTP induction). Synaptic responses, in which the amplitude of oEPSCs was < 8 pA, were determined to be failures. The failure rate, efficacy (mean EPSC amplitude including failures), and potency (mean EPSC amplitude excluding failures) were compared before (10 min baseline in the presence of D-AP5) with LTP (30 min after LTP induction). Spike probability was calculated as the number of spikes normalized to the total number of spikes per burst. Post-tetanic potentiation was calculated as the percentage of potentiation in the

mean of the 5 consecutive EPSC amplitudes following a burst of PF stimulation relative to the baseline EPSC amplitudes. Averaged representative traces included 10-30 consecutive individual responses.

2.8 Statistics

Statistical analysis was performed using OriginPro software (OriginLab, USA). The normality of distributions was assessed using the Shapiro-Wilk test. For samples with normal distributions, Student's unpaired and paired two-tailed t-tests were used to assess between-group and within-group differences, respectively. For samples that were not normally distributed, the non-parametric paired sample Wilcoxon signed rank test and Mann-Whitney U test were used. Differences among two or multiple samples were assessed by using one way or two-way ANOVA, followed by post hoc Tukey's test if necessary. Kolmogorov-Smirnov test was used for cumulative distributions. Statistical significance was set to $p < 0.05$ (***, **, and * indicates $p < 0.001$, $p < 0.01$ and $p < 0.05$, respectively). All values are reported as the mean ± s.e.m.

Chapter3. Results

3.1 Postsynaptic depolarization induces LTP at excitatory SuM-GC synapses

To investigate whether SuM-GC synapses undergo activity-dependent long-term plasticity, I performed whole-cell patch-clamp recordings from GCs in acute hippocampal slices. Because it is difficult to stimulate SuM inputs selectively by conventional electrical stimulation, I have used optogenetic approach. ChR2 can be selectively expressed to specific fibers by genetic approach, and the fibers can be activated by opening of ChR2, non-specific cation channels. To optogenetically activate SuM fibers in the DG, I stereotactically injected a Cre-dependent AAV to express channelrhodopsin-2 (ChR2) (AAV-DIO-ChR2(H134R)-eYFP) into the SuM of VGluT2-Cre mice as established previously (Fig. 5) (Y. Hashimotodani st al., 2018). By delivering blue light pulses, I recorded oEPSCs at SuM-GC synapses in the presence of picrotoxin to block inhibitory currents. I first tested whether excitatory SuM-GC synapses exhibited classical NMDAR-dependent Hebbian LTP. To test this, I applied a pairing protocol (200 light pulses at 2 Hz, paired with 0 mV postsynaptic depolarization), a commonly used protocol to induce Hebbian LTP (R. C. Malenka & R. A. Nicoll, 1999). I found that this pairing protocol induced robust LTP of SuM-GC oEPSCs (Fig. 6; control: 217 ± 23 % of baseline, $n = 10$, $p < 0.001$, paired t test). Unexpectedly, this LTP was not abolished by the NMDAR blocker D-AP5 (Fig. 6; D-AP5: 210 ± 26% of baseline, $n = 8$, $p < 0.001$, paired t test; control versus D-AP5: $p = 0.81$, unpaired t test). This result suggests that excitatory

SuM-GC synapses undergo NMDAR-independent LTP by the pairing protocol. To test whether NMDAR-independent LTP requires associative presynaptic and postsynaptic activity, I delivered solo presynaptic activation or postsynaptic depolarization. To our surprise, postsynaptic depolarization without presynaptic stimulation still caused LTP (Fig. 6; depol: 214 ± 21% of baseline, $n = 9$, $p < 0.001$, paired t test; control versus depol: $p = 0.89$, unpaired t test), whereas solo presynaptic stimulation failed to induce LTP (Fig. 6; pre only; 100 ± 6% of baseline, $n = 4$, $p > 0.98$, Wilcoxon signed rank test). These results suggest that postsynaptic depolarization alone can induce LTP at excitatory SuM-GC synapses.

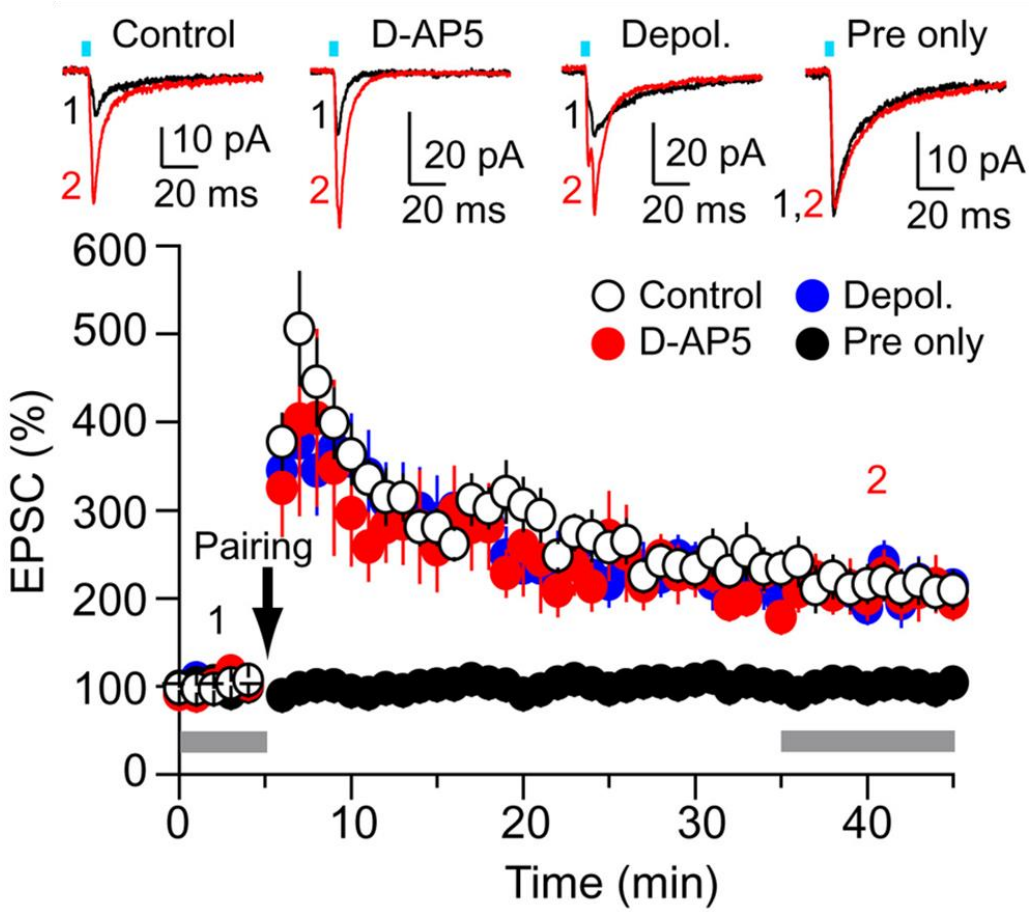

Figure 6. Postsynaptically induced LTP of SuM-GC EPSC

A pairing protocol (200 light pulses at 2 Hz, paired with 0-mV postsynaptic depolarization, arrow) induced robust LTP of SuM-GC oEPSCs (white circle). Same pairing protocol still induced LTP in the presence of 50

μM D-AP5 (red circle). Postsynaptic depolarization without presynaptic activity also induced LTP (blue circle), whereas presynaptic activity without postsynaptic depolarization failed to induce LTP (black circle). Representative traces, which correspond to the numbers in the time-course plot below (for this and all subsequent figures), are shown on the top. For this and all subsequent figures, blue bars indicate the time when blue light was delivered to slices. Gray bars indicate the time windows for quantification of the magnitude of LTP. Here and in all figures, the magnitude of LTP was measured by comparing baseline responses with the last 10-min responses after LTP induction shown in each experiment. Data are presented as mean ± SEM.

Several previous studies have demonstrated that postsynaptic depolarization induces LTP at CA3-CA1 synapses of the hippocampus (L. Aniksztejn & Y. Ben-Ari, 1991; L. M. Grover & T. J. Teyler, 1990; Y. Y. Huang & R. C. Malenka,1993; H. K. Kato et al., 2009). To test whether excitatory SuM-GC synapses also undergo similar non-Hebbian plasticity by a much shorter duration of postsynaptic depolarization than the pairing protocol (100 s in Fig. 6), I applied repeated depolarizing pulses (2 s duration repeated 10 times every 5 s from a holding potential of –60 mV to 0 mV). I found that depolarizations of GCs induced robust LTP of excitatory SuM-GC transmission (depol-eLTP), which peaked within 10 min and maintained stable potentiation for up to 60 min (Fig. 7A; 196 ± 19% of baseline, $n = 13$, $p < 0.001$, paired t test). In subsequent experiments, I used the repeated depolarizing pulses as the standard induction protocol for depol-eLTP. The magnitude of the depol-eLTP depended on the number of depolarizing pulses (Fig. 7B). To test whether depol-eLTP could be induced by physiologically relevant GC activity, I applied burst APs in GCs at the theta frequency, which mimics the *in vivo* firing pattern of GCs that show sparse activity with intermittent burst firing at theta oscillations (M. Diamantaki st al., 2016; A. J. Pernía-Andrade & P. Jonas, 2014; D. Vandael et al., 2020; O. Caillard et al., 1999). I found that AP

firing in GCs (10 bursts of APs at 5 Hz, repeated 5 times every 5 s) in current-clamp mode using a more physiological K^+-based intracellular solution induced robust LTP (Fig. 7C; 172 ± 17% of baseline, n = 8, $p < 0.01$, paired t test). Consistent with the NMDAR-independence of LTP induced by the pairing protocol (Fig. 6), depol-eLTP induced by repeated depolarizing pulses was also intact in the presence of D-AP5 (Fig. 8; 202 ± 27% of baseline, n = 10, $p < 0.01$, paired t test), suggesting an NMDAR-independent mechanism for depol-eLTP. These results indicate that excitatory SuM-GC synapses express an NMDAR-independent form of non-Hebbian LTP following postsynaptic depolarization.

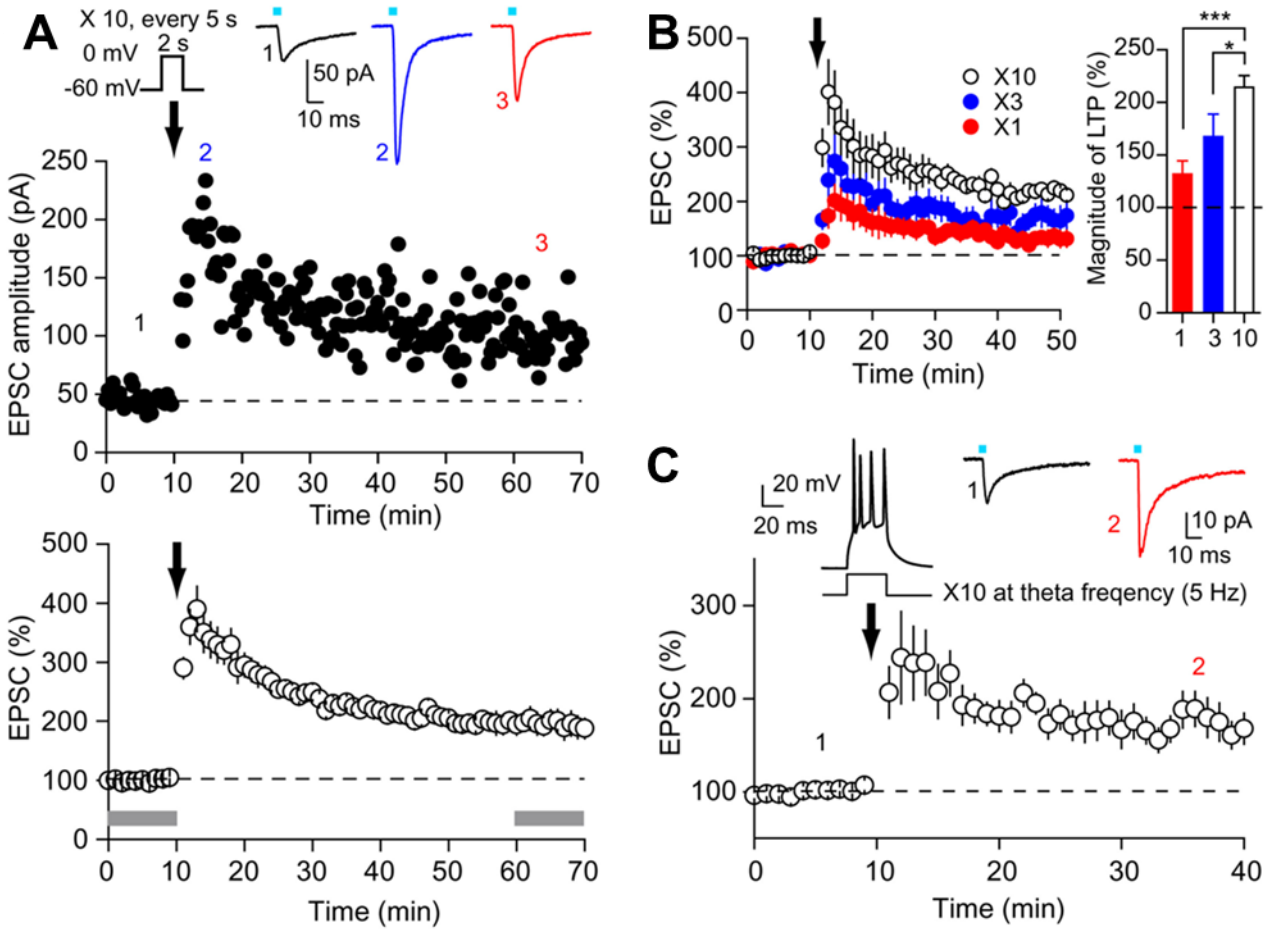

Figure 7. Physiological characterization of LTP

(A) Representative experiment (Upper) and summary plot (Lower) show repeated depolarizations (2-s

duration repeated 10 times every 5 s, arrow) of GCs induced robust LTP of SuM-GC oEPSCs. (B) The magnitude of depol-eLTP depends on the number of depolarizing pulses. Each protocol was applied to the different cells. Summary data at right shows the magnitude of LTP induced by different numbers of depolarizing pulses (once, 132 ± 13% of baseline, n = 11; three times, 167 ± 22% of baseline, n = 11; 10 times, 214 ± 11% of baseline, n = 11). One-way ANOVA, $P < 0.001$, Tukey's post hoc test *$P < 0.05$; ***$P < 0.001$. (C) Burst APs in GCs at θ frequency (10 bursts of 40-ms current injection, which elicited three to four APs, at 5 Hz, repeated five times every 5 s, arrow) induced LTP. (Inset) Example trace of a single burst APs. Gray bars in A indicate the time windows for quantification of the magnitude of LTP.

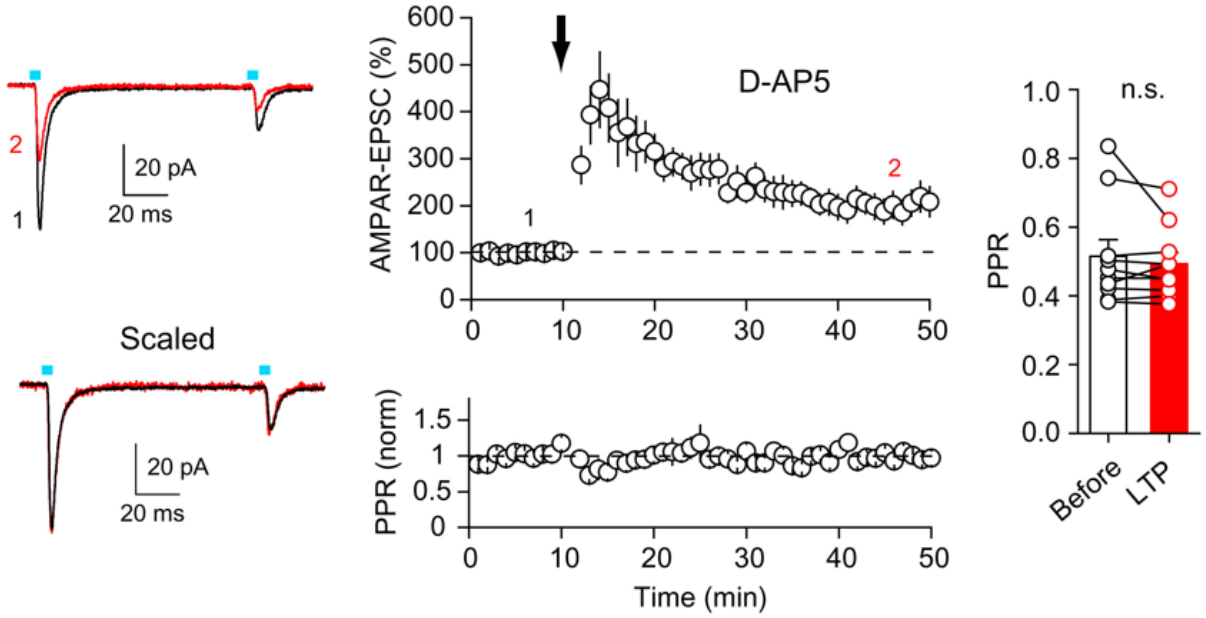

Figure 8. NMDA independent LTP of SuM-GC EPSCs

Depol-eLTP was normally induced by repeated postsynaptic depolarizations (arrow) in the presence of 50 μM D-AP5. PPR was not changed after induction of depol-eLTP. (Left) Representative traces; (Center) time course summary plot of depol-eLTP (Upper) and normalized PPR (Lower); (Right) summary plot of PPR.

3.2 Depolarization of GCs exhibits postsynaptic LTP of SuM-GC AMPAR-mediated transmission but not GABAergic co-transmission

I next tested whether depol-eLTP was expressed pre- or post-synaptically. By monitoring the paired-pulse ratio (PPR), a commonly used index of presynaptic change. Specifically, the PPR is known to be inversely correlated to presynaptic release probability and postsynaptic changes give

rise to no change in the PPR. I found that the PPR was not changed after induction of depol-eLTP of SuM-GC AMPAR-oEPSCs (before: 0.52 ± 0.05; LTP: 0.49 ± 0.03, n = 10, p = 0.49, Wilcoxon signed rank test) (Fig.8). Moreover, depol-eLTP increased the amplitude, but not the frequency, of asynchronous SuM-GC oEPSCs in the presence of strontium (Fig. 9A; amplitude: before: 9.7 ± 0.24 pA; after: 14.1 ± 0.44 pA, n = 7, $p < 0.001$, paired t test; frequency: before: 3.7 ± 0.31 Hz; after: 3.7 ± 0.34 Hz, n = 7, p = 0.92, paired t test). Frequency and amplitudes of asynchronous release should reflect pre- and postsynaptic changes respectively, in principle. These results suggest that depol-eLTP is likely expressed postsynaptically. To further test the potential involvement of presynaptic changes during depol-eLTP, I investigated the effects of depolarizing pulses on NMDAR-mediated synaptic transmission at SuM-GC synapses. If depol-eLTP is caused by a long-lasting increase in glutamate release, both AMPAR- and NMDAR-mediated synaptic transmission will be equally potentiated. I found that pharmacologically isolated SuM-GC NMDAR-oEPSCs were detectable at –60 mV, even in the presence of 1.3 mM Mg^{2+} (Fig. 9B). This observation allows us to deliver the same magnitude of depolarization (from –60 to 0 mV) as AMPAR-oEPSCs for monitoring NMDAR-oEPSCs. Unlike AMPAR-oEPSCs, NMDAR-oEPSCs did not show LTP following postsynaptic depolarizations (Fig. 9C; 101 ± 4% of baseline, n = 10, p = 0.85, paired t test). These results also suggest that depol-eLTP is expressed postsynaptically.

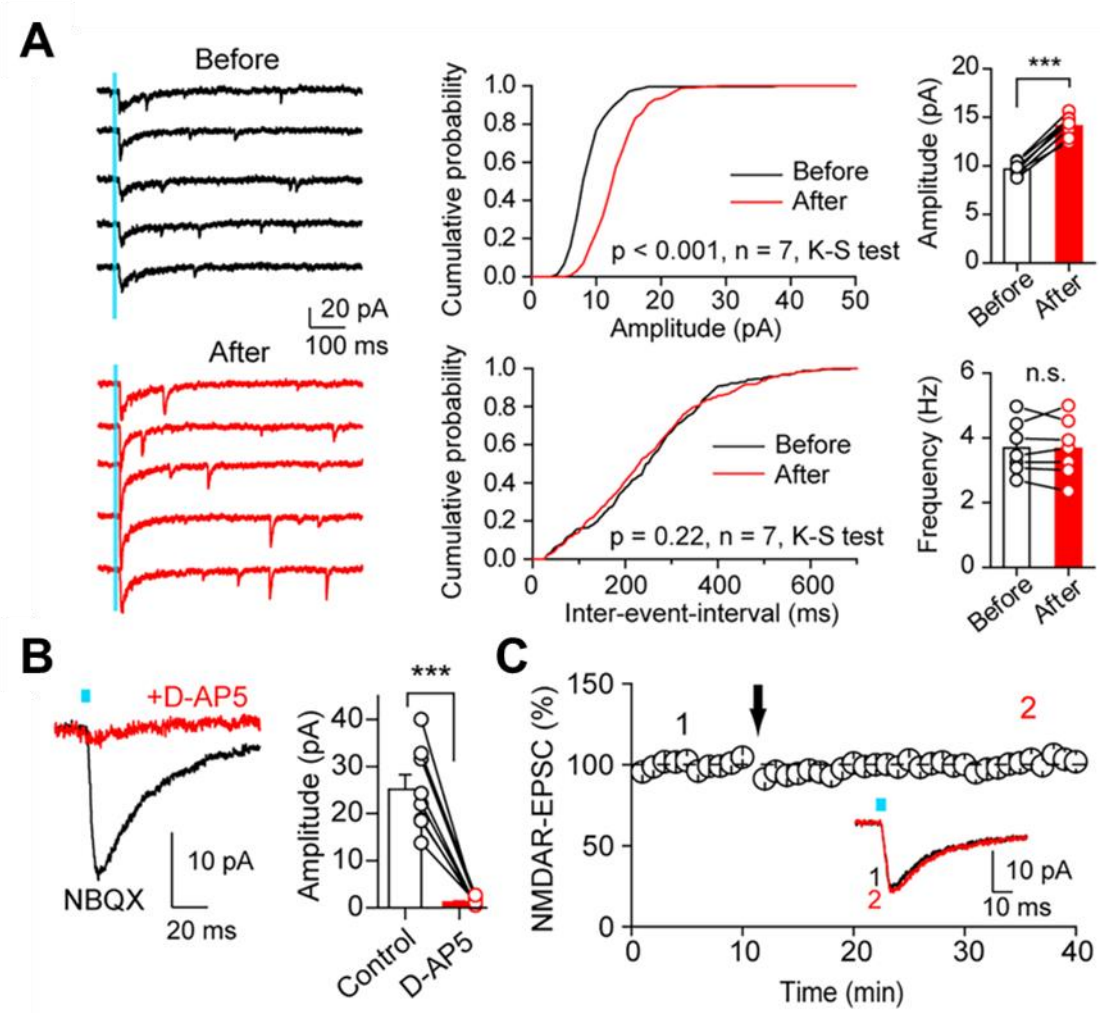

Figure 9. Depol-eLTP at SuM-GC synapses is expressed postsynaptically

(A) The effect of postsynaptic depolarizations on asynchronous synaptic responses in the presence of Sr^{2+}. Representative traces (Left) of asynchronous SuM-GC oEPSCs before (10-min baseline) and after induction of depol-eLTP (20 min after GC depolarizations). (Center) Cumulative amplitude and interevent interval distributions of asynchronous events obtained before and after depol-eLTP induction. (Right) Amplitude and frequency summary plots of asynchronous events obtained before and after depol-eLTP induction. For induction of depol-eLTP, extracellular Sr^{2+} solution was replaced by normal artificial cerebrospinal fluid (ACSF) containing Ca^{2+} after 10-min baseline. After confirming the induction of depol-eLTP, extracellular solution was returned to Sr^{2+}-containing ACSF. (B) SuM-GC NMDAR-oEPSCs were recorded at –60 mV in the presence of 10 μM NBQX and 100 μM picrotoxin (black trace). NMDAR-oEPSCs were completely blocked by 50 μM D-AP5 (red trace, n = 8, P < 0.001, paired t test). (C) The depol-eLTP induction protocol failed to induce LTP of NMDAR-oEPSCs. Data are presented as mean ± SEM; ***P < 0.001. n.s., not significant.

In addition to excitatory synapses, several studies have demonstrated that postsynaptic depolarization induces LTP at inhibitory synapses in several brain regions (O. Caillard et al., 1999; M. Kano1et al.,1992; T. Kurotani et al., 2008; J. Lourenço et al., 2014; A. R. Sieber 2013). I examined the effects of postsynaptic depolarization on GABAergic co-transmission. Using an intracellular solution containing a high concentration of Cl^- (calculated E_{Cl^-} = –20 mV), I recorded optically evoked inhibitory postsynaptic currents (oIPSCs) from GCs as inward currents at –60 mV. Unlike AMPAR-oEPSCs, SuM-GC oIPSCs did not exhibit LTP by the depol-eLTP induction protocol (Fig. 10; 105 ± 10% of baseline, n = 12, p = 0.72, Wilcoxon signed rank test), but showed transient potentiation (Fig. 10; 0-5 min after depolarization; 129 ± 47% of baseline, n = 12, $p < 0.01$, Wilcoxon signed rank test). Even stronger depolarizing pulses (20 times) elicited only transient potentiation (Fig. 10; 0-5 min after depolarization; 132 ± 14 % of baseline, n = 6, $p < 0.05$, paired t test), but not LTP of oIPSCs (Fig. 10; 101 ± 8% of baseline, n = 6, p = 0.87, paired t test). As PPR was not changed during this transient potentiation (before: 0.56 ± 0.03; after: 0.55 ± 0.02, n = 6, p = 0.52, paired t test), postsynaptic change could be transiently induced after depolarization. Altogether, these results indicate that depolarization of GCs selectively induces a postsynaptic form of LTP of glutamatergic, but not GABAergic, co-transmission at SuM-GC synapses. Thus, selective expression of LTP at excitatory SuM-GC synapses increases the excitatory drive of glutamate/GABA co-release synapses.

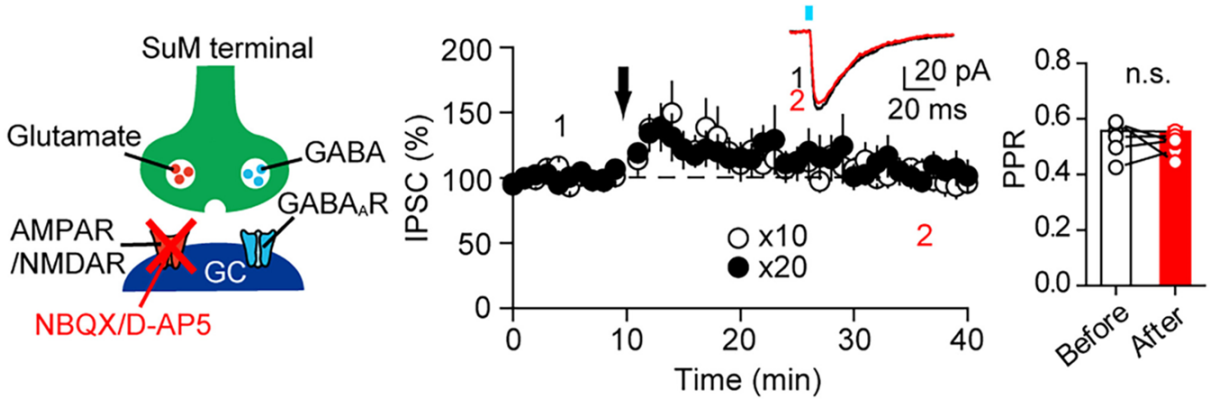

Figure 10. GABAergic cotransmission is intact following GC depolarization

(Left) Schematic diagram illustrating blockade of glutamatergic transmission by NBQX and D-AP5 leaving GABAergic cotransmission intact at SuM-GC synapses. (Center) Repetitive postsynaptic depolarizations (open circles: 10 pulses; filled circles: 20 pulses) failed to induce LTP of SuM-GC oIPSCs. (Right) PPR of SuM-oIPSCs before and after (0 to 5 min after depolarization) 20 depolarizing pulses. Data are presented as mean ± SEM; ***P < 0.001. n.s., not significant.

3.3 Synapse type- and target cell-specificity of depol-eLTP

Given that postsynaptic depolarization is supposed to cause neuron-wide Ca^{2+} influx at least near somatic region, other inputs besides SuM may elicit LTP by the depolarization of GCs. To test this possibility, the medial perforant-path (MPP), the main excitatory inputs from the entorhinal cortex (D. G. Amaral et al., 2007), was extracellularly stimulated, and electrically evoked MPP-EPSCs and optically evoked SuM-oEPSCs were alternately recorded from the same GC (Fig. 11A). I found that the depol-eLTP induction protocol failed to induce LTP at MPP-GC synapses, while SuM-GC synapses exhibited LTP (Fig. 11B; SuM: 198 ± 17% of baseline, n = 11, p < 0.001, paired t test; MPP: 112 ± 11% of baseline, n = 11, p = 0.27, paired t test).

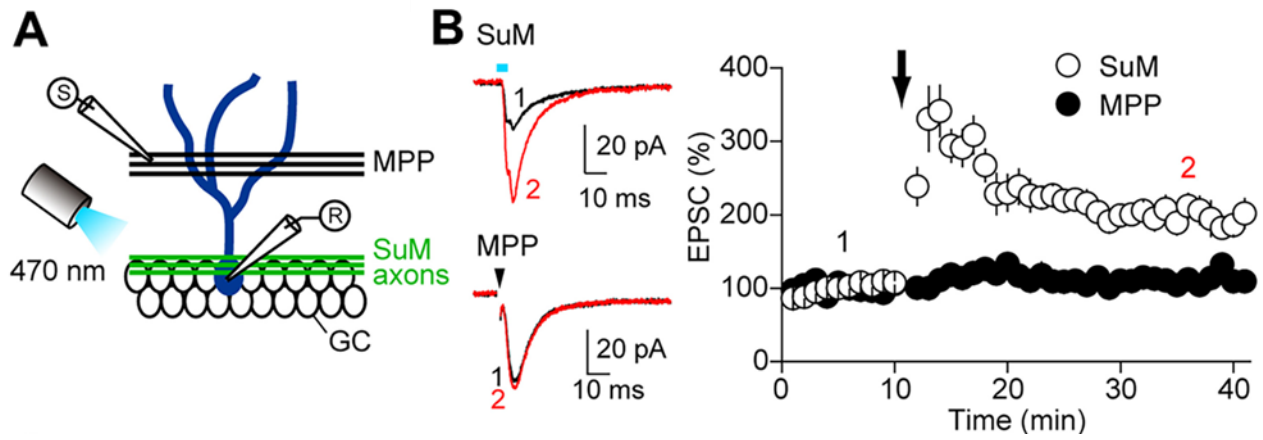

Figure 11. Input-specificity of depol-eLTP

(A) Schematic drawing of recording of electrically evoked MPP-EPSCs and optically evoked SuM-EPSCs from the same GC. Each input was alternately stimulated every 10 s. (B) Repetitive depolarizing pulses of GCs (arrow) elicited LTP of SuM-oEPSCs but not MPP-EPSCs. Data are presented as mean ± SEM.

I further examined whether depol-eLTP is SuM projection target cell-specific. Hasimotodani et al. (2018) previously demonstrated that SuM neurons also make monosynaptic connections to GABAergic INs in the DG. To examine whether SuM-IN synapses undergo depol-eLTP, I recorded SuM-IN oEPSCs from INs in the DG (See Methods) (Fig. 12A). I found that the depol-eLTP induction protocol failed to induce LTP of SuM-IN oEPSCs, whereas SuM-GC oEPSCs exhibited LTP in interleaved slices (Fig. 12B; IN: 94 ± 6% of baseline, n = 10, p = 0.36, paired t test; GC: 189 ± 29% of baseline, n = 9, $p < 0.01$, paired t test). In addition to the DG, the CA2 region is another main target of SuM afferents (L. Haglund et al., 1984; R. P. Vertes., 1992; K. Kohara et al., 2014). I tested whether depolarization of CA2 pyramidal neurons could induce LTP at SuM-CA2 pyramidal neuron synapses. In agreement with recent reports (S. Chen et al., 2020; V. Robert et al., 2021), light activation of the SuM fibers evoked oEPSCs recorded from CA2 pyramidal neurons (19.4 ± 3.4 pA, n = 10) (Fig. 12C and D). In contrast to DG GCs, However, I

found that depolarizations of CA2 pyramidal neurons did not trigger LTP at SuM-CA2 pyramidal neuron synapses (Fig. 12D; 100 ± 12% of baseline, n = 10, p = 0.96, paired t test). Taken together, these results indicate that SuM inputs express depol-eLTP in a target cell-specific manner, and GCs targeted by the SuM afferents exclusively exhibit depol-eLTP.

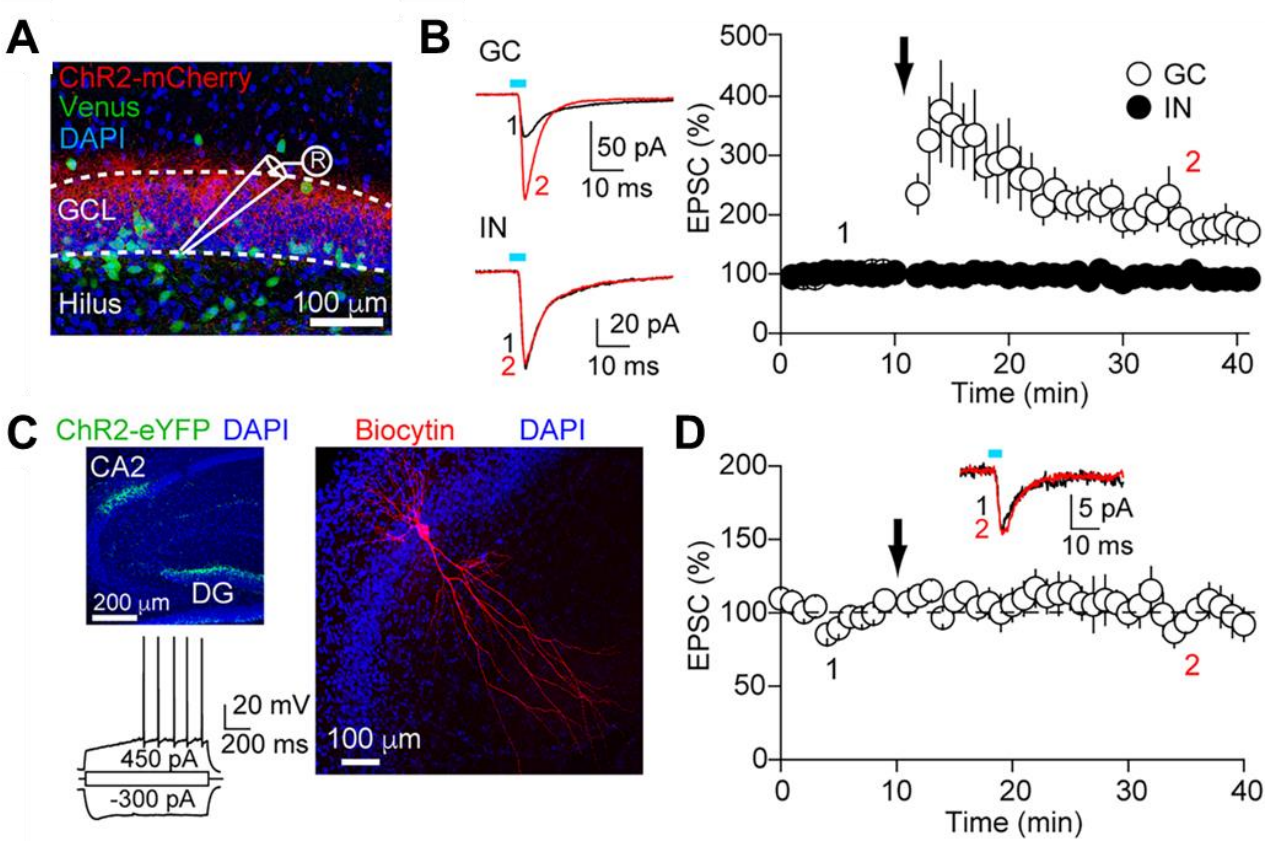

Figure 12. Target cell-specificity of depol-eLTP

(A) Experimental diagram. A confocal image of DG obtained from a VGluT2-Cre/VGAT-Venus mouse expressing ChR2(H134R)-mCherry in the SuM axons. Whole-cell recording was performed from a $Venus^+$ IN. (B) Repetitive depolarizations of INs failed to induce LTP, while interleaved recordings from GCs exhibited depol-eLTP. (C, Upper Left) ChR2(H134R)-eYFP-expressing SuM axons project to CA2 in addition to the DG. (Right) A confocal image of a biocytin-filled CA2 pyramidal neuron. (Lower Left) Intrinsic electrophysiological properties in responses to 1-s current steps in a CA2 pyramidal neuron. As typical characteristics of CA2 pyramidal neurons, delayed APs and minimal sag were elicited by a positive and negative current injection, respectively. (D) The depol-eLTP induction protocol did not induce LTP at SuM-CA2 pyramidal neuron synapses. Data are presented as mean ± SEM.

3.4 Depol-eLTP requires postsynaptic Ca^{2+} increases, CaMKII and SNARE-dependent exocytosis

Next, I investigated the postsynaptic mechanisms underlying depol-eLTP. As postsynaptic depolarization triggers postsynaptic Ca^{2+} influx, I examined whether postsynaptic Ca^{2+} influx is necessary for the induction of depol-eLTP. Intracellular loading GCs with the Ca^{2+} chelator BAPTA (20 mM) completely abolished depol-eLTP (Fig. 13A; 104 ± 7% of baseline, n = 11, $p < 0.01$, compared to control, unpaired t test). Voltage gated Ca^{2+} channels are a candidate for the main source of postsynaptic Ca^{2+} entry. Ca^{2+} channels are classified as P/Q, N, R and L type, according to pharmacological and molecular dissection. Among them, bath application of the L-type VDCC blocker nifedipine (30 μM) blocked depol-eLTP (Fig. 13A; 93 ± 10% of baseline, n = 10, $p < 0.001$, compared to control, Mann-Whitney U test). I excluded the involvement of Ca^{2+} release from internal stores in depol-eLTP, as pretreatment of slices with cyclopiazonic acid (CPA, 30 μM), a manipulation to deplete intracellular Ca^{2+} stores, did not block the induction of depol-eLTP (Fig. 13B; 227 ± 36 % of baseline, n = 5, $p = 0.67$, compared to control, unpaired t test). These results indicate that depol-eLTP at SuM-GC synapses requires postsynaptic Ca^{2+} influx through L-VDCCs.

Several types of protein kinases, including PKA, PKC, and CaMKII, contribute to LTP induction (B. E. Herring & R. A. Nicoll, 2016; J. Lisman et al., 2012; R. Malinow et al., 1989; P. V. Nguyen & N. H. Woo, 2003). I examined whether the inhibitors of these kinases could block depol-eLTP. I found that neither the PKA inhibitor H89 (10 μM) nor the PKC inhibitor Gö6983 (1 μM)

blocked the induction of depol-eLTP (Fig. 13C and D; H89: 186 ± 33% of baseline, n = 8, p = 0.72, compared to control, unpaired t test; Gö6983: 221 ± 16% of baseline, n = 7, p = 0.91, compared to control, unpaired t test). Next, I examined the involvement of CaMKII in depol-eLTP. Bath application of the CaMKII inhibitor KN-93 (10 μM) abolished depol-eLTP (Fig. 13E; 114 ± 12% of baseline, n = 6, $p < 0.05$, compared to control, unpaired t test). To determine the potential contribution of postsynaptic CaMKII activity in depol-eLTP, I applied the specific CaMKII peptide inhibitor autocamtide-2-related inhibitory peptide (AIP, 10 μM) via a patch pipette. Loading GCs with AIP blocked depol-eLTP (Fig. 13F; 111 ± 13% of baseline, n = 5, $p < 0.05$, compared to control, unpaired t test). These results clearly indicate that depol-eLTP requires postsynaptic CaMKII activity.

I next investigated the postsynaptic expression mechanisms of depol-eLTP. Growing evidence indicates that the insertion of AMPARs via SNARE-dependent exocytosis in the postsynaptic plasma membrane is necessary for canonical NMDAR-dependent LTP at CA3-CA1 synapses (B. E. Herring & R. A. Nicoll, 2016; J. Lisman et al., 2012; D. Choquet, 2018). I tested whether similar mechanisms could mediate depol-eLTP. I found that postsynaptic loading with N-ethylmaleimide (NEM, 500 μM) and botulinum toxin-A (BoTx, 200 ng/mL), both of which inhibit SNARE-dependent exocytosis (P. M. Lledo et al., 1998), abolished depol-eLTP (Fig. 13G and H; NEM: 102 ± 13% of baseline, n = 7, $p < 0.01$, compared to control, unpaired t test; BoTx: 87 ± 17% of baseline, n = 7, $p < 0.01$, compared to control, unpaired t test). These results suggest that depol-

eLTP requires the exocytosis of AMPAR-containing vesicles.

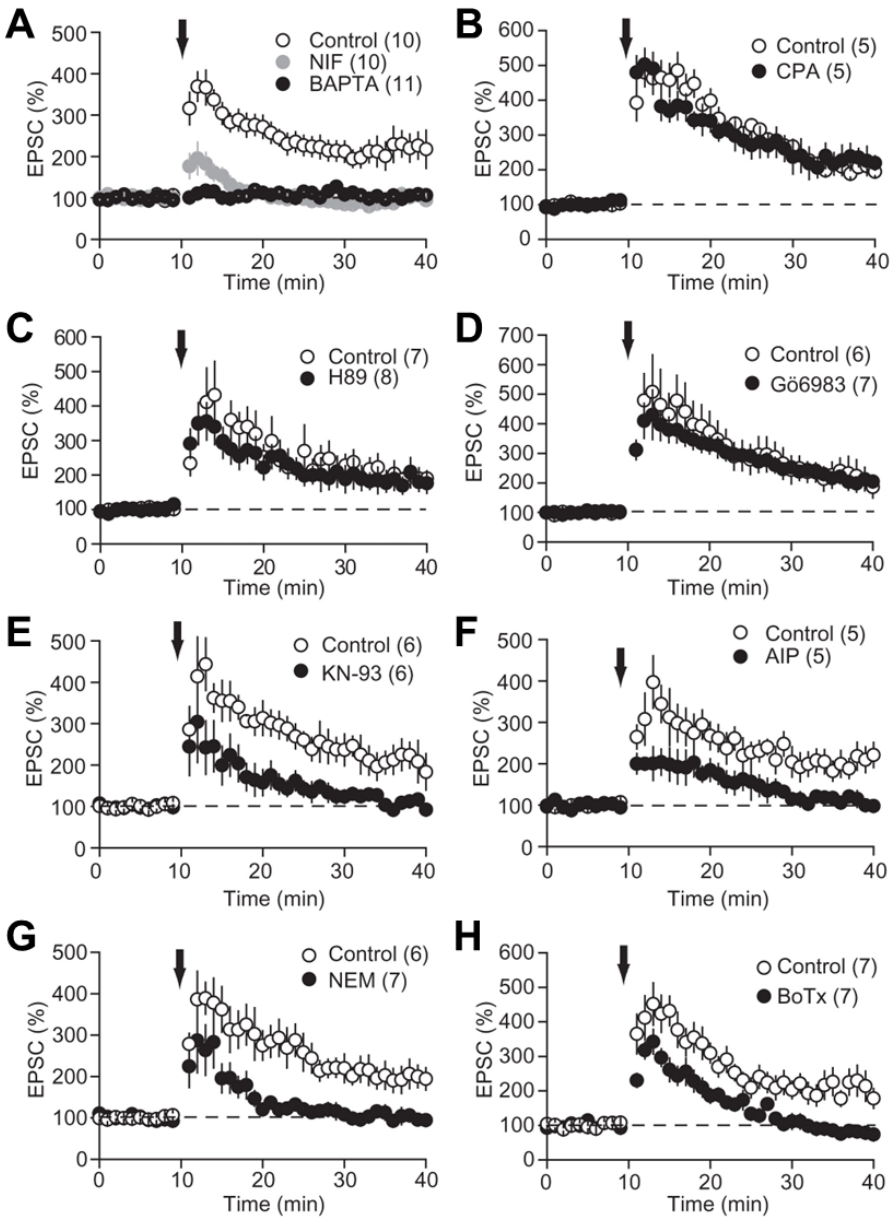

Figure 13. Molecular mechanisms underlying depol-eLTP

(A) Depol-eLTP required a postsynaptic Ca^{2+} increase through L-VDCCs. Postsynaptic loading with 20 mM BAPTA failed to induce depol-eLTP. Postsynaptic depolarizations (arrow) abolished depol-eLTP in the presence of 30 μM nifedipine. Numbers in parentheses, here and in all figures, indicate the number of cells. (B) Depletion of intracellular Ca^{2+} stores by CPA (30 μM) had no effect on depol-eLTP. (C) Bath application of the PKA inhibitor H89 (10 μM) had no effect on depol-eLTP. (D) Bath application of the PKC inhibitor Gö6983 (1 μM) had no effect on depol-eLTP. (E) Bath application of the CaMKII inhibitor KN-93 (10 μM) abolished depol-eLTP. (F) Postsynaptic loading with the CaMKII inhibitor AIP (10 μM) abolished depol-eLTP. (G) Depol-eLTP was blocked by postsynaptic loading with NEM (500 μM). (H) Postsynaptic loading with BoTx (200 ng/mL) abolished depol-eLTP, while heat-inactivated BoTx (control) normally induced depol-eLTP. Data are presented as mean ± SEM.

3.5 Depolarization of GCs may induce NMDAR-independent unsilencing of SuM-GC synapses

It is widely accepted that silent synapses, which contain NMDARs but no functional AMPARs, provide synaptic substrates for LTP in the young brain, and AMPAR unsilencing (insertion of AMPARs into the postsynaptic membrane) by correlated pre- and postsynaptic activity is implicated in postsynaptic mechanisms for NMDAR-dependent form of LTP (G. A. Kerchner & R. A. Nicoll, 2008). Because depol-eLTP is expressed postsynaptically and requires exocytosis of AMPARs, I sought to determine whether silent synapses could also exist at SuM-GC synapses, and postsynaptic depolarization could cause synapse unsilencing. By measuring the NMDAR/AMPAR ratio, I found that SuM-GC synapses showed higher NMDAR/AMPAR ratio than those of SuM-IN synapses (Fig. 14A). The results may mean that AMPARs are not copious at SuM-GC synapses and imply that they may contain a large fraction of NMDAR-only synapses. Because NMDA receptors are not activated around resting potential, the results may suggest that SuM-GC synapses contain more silent synapses than conventional synapses. Usually, for detecting silent synapses, no evoked AMPAR-EPSCs by subthreshold fiber stimulation are recorded at negative membrane potentials, and then NMDAR-EPSCs are recorded at positive membrane potentials (G. A. Kerchner & R. A. Nicoll, 2008). However, under our experimental conditions, holding GCs at positive membrane potentials to record NMDAR-oEPSCs causes an influx of Ca^{2+}, which can induce LTP of AMPAR-oEPSCs at SuM-GC synapses. To avoid this issue, I recorded both AMPAR- and NMDAR-oEPSCs

at –60 mV, as recording of NMDAR-oEPSCs at –60 mV is feasible at SuM-GC synapses (Fig. 9B). In a subset of cells, when the intensity of light illumination was reduced, I observed oEPSCs, which showed a slow rise time (Fig. 14B, and see Methods). Following bath application of D-AP5, light illumination failed to evoke any responses, suggesting that baseline responses were mediated by NMDARs without AMPARs. Under these conditions, delivering the depol-eLTP induction protocol resulted in the long-lasting appearance of AMPAR-oEPSCs that were associated with a significant decrease in failure rate (Fig. 14B and C; before: 100%; LTP: 6.8 ± 1.8%, $n = 9$, $p < 0.01$, Wilcoxon signed rank test) and an increase in efficacy (mean EPSC amplitude including failures) (Fig. 14C; before: 1.7 ± 0.2 pA; LTP: 16.5 ± 1.0 pA, $n = 9$, $p < 0.001$, paired t test) and potency (mean EPSC amplitude excluding failures) (Fig. 14C; before: 0 pA; LTP: 17.5 ± 1.0 pA, $n = 9$, $p < 0.01$, Wilcoxon signed rank test). In 6 out of 9 cells, I successfully recorded NMDAR-oEPSCs 30 min after washout of D-AP5 and confirmed that the depol-eLTP induction protocol did not change the amplitude of NMDAR-oEPSCs (Fig. 14C; before: 14.9 ± 1.6 pA; LTP: 14.3 ± 1.9 pA, $n = 6$, $p = 0.48$, paired t test). These results indicate that GC depolarization can cause NMDAR-independent synapse unsilencing through the incorporation of AMPARs into synapses.

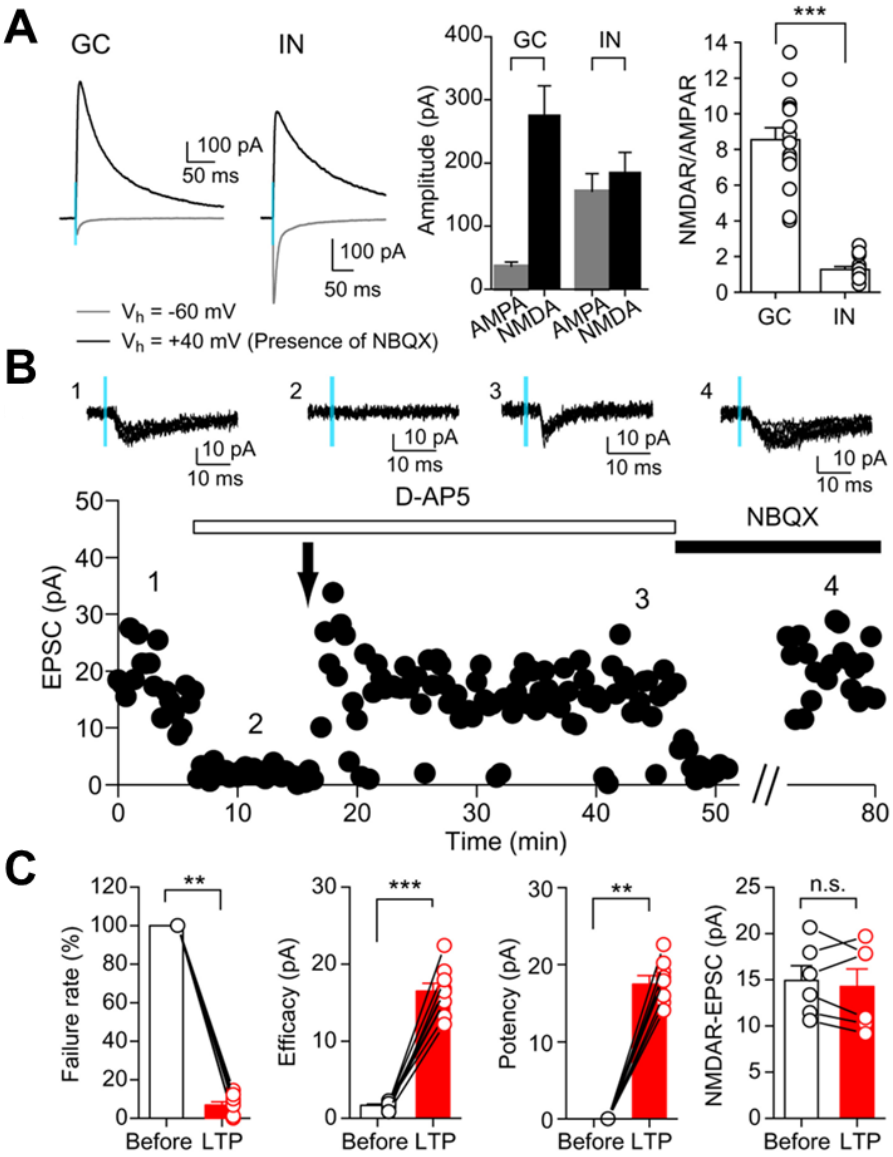

Figure 14. High NMDAR/AMPAR ratio in GCs and synapse unsilencing induced by depolarization of GCs

(A) Marked difference in the NMDAR/AMPAR ratios at SuM-GC and SuM-IN synapses. (Left) oEPSCs recorded from GCs and INs at −60 mV and +40 mV. oEPSCs at +40 mV were recorded in the presence of 10 μM NBQX. (Center) Quantification of the amplitudes of AMPAR- and NMDAR-mediated currents recorded from GCs and INs. (Right) Summary data showing the NMDAR/AMPAR ratios (GC: 8.5 ± 0.67, n = 17; IN: 1.3 ± 0.16, n = 15, $P < 0.001$, unpaired t test). (B) Representative experiment of sample traces (Upper: six sweeps overlaid) and time course (Lower). oEPSCs evoked by weak light illumination at −60 mV showed slow rise time and were completely blocked by 50 μM D-AP5. Under this condition (no detectable oEPSCs), repetitive postsynaptic depolarizing pulses (arrow) elicited appearance of oEPSCs. NBQX (10 μM) was applied at the end of experiment to verify the response was mediated by AMPARs. After washout of D-AP5 in the presence of NBQX, NMDAR-oEPSCs were recovered without any potentiation. (C) Summary plots demonstrating that synapse unsilencing was associated with a significant decrease in failure rate, increase in efficacy and potency and no significant change in NMDAR-oEPSCs. Data are presented as mean ± SEM; $^{**}P < 0.01$, $^{***}P < 0.001$. n.s., not significant

3.6 MPP inputs heterosynaptically trigger depol-eLTP

Thus far, I demonstrate that Ca^{2+} influx into GCs by their depolarization induces depol-eLTP. What is the input source for depolarizing GCs to trigger depol-eLTP under physiological conditions? Given that solo SuM inputs are too weak to excite GCs (Y. Hashimotodani et al., 2018), other strong inputs, rather than SuM inputs, could effectively depolarize GCs and then heterosynaptically trigger depol-eLTP. Because the perforant-path (PP) derived from the entorhinal cortex is the major input source to excite GCs (A. J. Pernía-Andrade & P. Jonas, 2014; A. Bragin et al., 1995), I hypothesized that GC firing driven by PP inputs could trigger depol-eLTP. To address this possibility, I employed theta-burst stimulation (TBS), which is often used as an LTP-induction paradigm corresponding to the physiologically relevant activity patterns of GCs (C. Schmidt-Hieber et al., 2004; S. Ge et al., 2007; W. E. Skaggs et al., 1996; C. Pavlides wt al., 1988), to evoke burst GC firing (Fig. 15A). After obtaining a 5 min baseline of SuM-GC oEPSCs in voltage-clamp mode, I switched to the current-clamp mode to allow the cell to generate APs and applied TBS to the MPP (Fig. 15B). The recording was then switched back into the voltage-clamp mode, and SuM-GC oEPSCs were monitored. I found that TBS of the MPP induced robust LTP at SuM-GC synapses (Fig. 15B and C; 196 ± 16% of baseline, $n = 6$, $p < 0.001$, paired t test). This LTP was completely blocked by postsynaptic application of BAPTA (Fig. 15C; 101 ± 10% of baseline, $n = 5$, $p < 0.001$, compared to control, unpaired t test), suggesting that Ca^{2+} influx driven by TBS of the MPP is required for the induction of LTP. Similar to depol-eLTP, TBS-induced LTP was normally

induced in the presence of D-AP5 (198 ± 24% of baseline, n = 8, $p < 0.05$, Wilcoxon signed rank test) and blocked by 10 μM KN-93 (117 ± 11% of baseline, n = 5, $p = 0.11$, paired t test) (Fig. 15D). Together, these results indicate that LTP at excitatory SuM-GC synapses can be heterosynaptically induced by MPP-mediated burst GC firing.

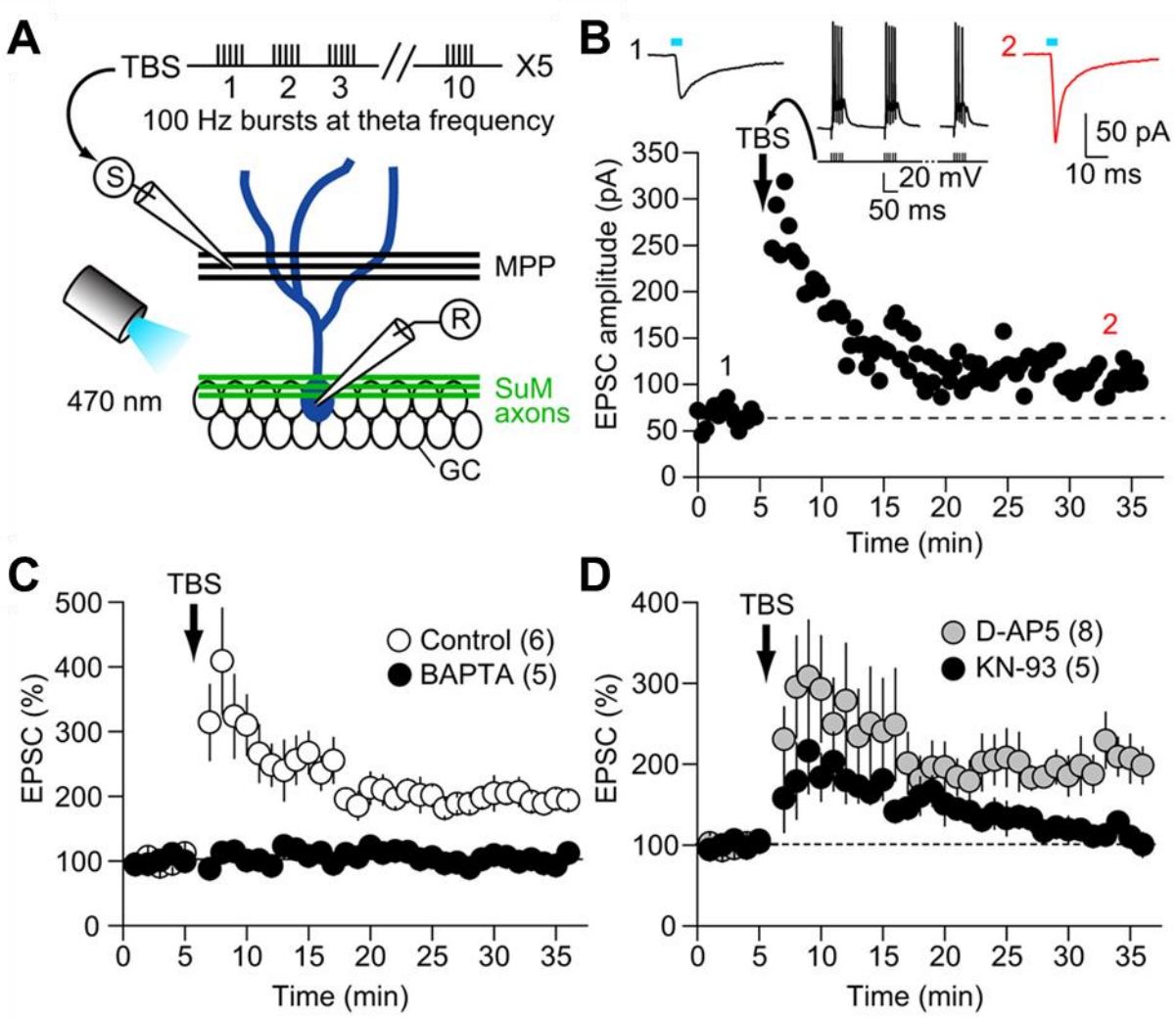

Figure 15. TBS of MPP inputs heterosynaptically induces eLTP at SuM-GC synapses

(A) Schematic drawing of recording configuration. MPP inputs were electrically stimulated by a glass electrode and ChR2-eYFP expressing SuM fibers were optically stimulated by a blue light pulse. For induction of LTP, MPP inputs were stimulated by TBS. (B) Representative experiment showing that TBS of MPP inputs (vertical arrow) induced robust LTP of SuM-GC oEPSCs. (Inset) APs during TBS. (C) Summary data showing that TBS-induced LTP was completely blocked by intracellular loading of BAPTA (20 mM). (D) TBS-induced LTP was induced in the presence of D-AP5 (50 μM) but blocked by bath application of KN93 (10 μM). Data are presented as mean ± SEM.

3.7 SuM inputs generate AP firing in GCs after induction of depol-eLTP

Given that GC burst-firing selectively potentiates glutamatergic, but not GABAergic, co-transmission at SuM-GC synapses, depol-eLTP dramatically increases the excitatory drive of SuM inputs. Therefore, highly potentiated SuM glutamatergic inputs could generate AP firing in GCs even if SuM inputs cannot drive APs under basal conditions (Y. Hashimotodani et al., 2018). Previous studies have reported that the resting membrane potential of mature GCs is more negative than E_{GABA} (P. H. Chiang et al., 2012; J. F. Sauer et al., 2012; K. J. Staley & I. Mody, 1992). Accordingly, GABAergic action is depolarizing under resting conditions. To mimic this condition, I held the membrane potential between −80 and −85 mV (referred to as −80 mV) in the current-clamp mode with inhibition intact. Under these conditions, I found that brief-burst light illumination of SuM inputs (4 pulses at 20 Hz) failed to induce APs in GCs (Fig. 16A). After a stable 5 min baseline, I delivered the depol-eLTP protocol under the voltage-clamp mode. Remarkably, the same burst stimulation triggered spike generation in 29% (7 of 24 cells) of GCs after LTP induction (Fig. 16A), suggesting that an increase in the excitatory drive of SuM inputs associated with depol-eLTP triggers GC firing. I next examined how GABAergic co-transmission contributes to SuM input-evoked spike generation following LTP induction. Under blockade of inhibition by picrotoxin, in which brief-burst light illumination evoked no spikes, I found that LTP induction triggered a significant increase in spike generation (44 %, 11 of 25 cells) compared with inhibition intact (Fig. 16B, C, and E). These results suggest that GABAergic co-transmission

negatively regulates glutamatergic SuM input-evoked GC firing. Given that glutamate and GABA are simultaneously released from the same SuM inputs, the inhibitory action of GABA is expected to be exerted via shunting inhibition (P. H. Chiang et al., 2012; A. T. Gulledge & G. J. Stuart, 2003). In both conditions, most spikes were confined to the early time period (~10 min) after depol-eLTP induction, and there was no difference in the distribution of spike numbers (Fig. 16D).

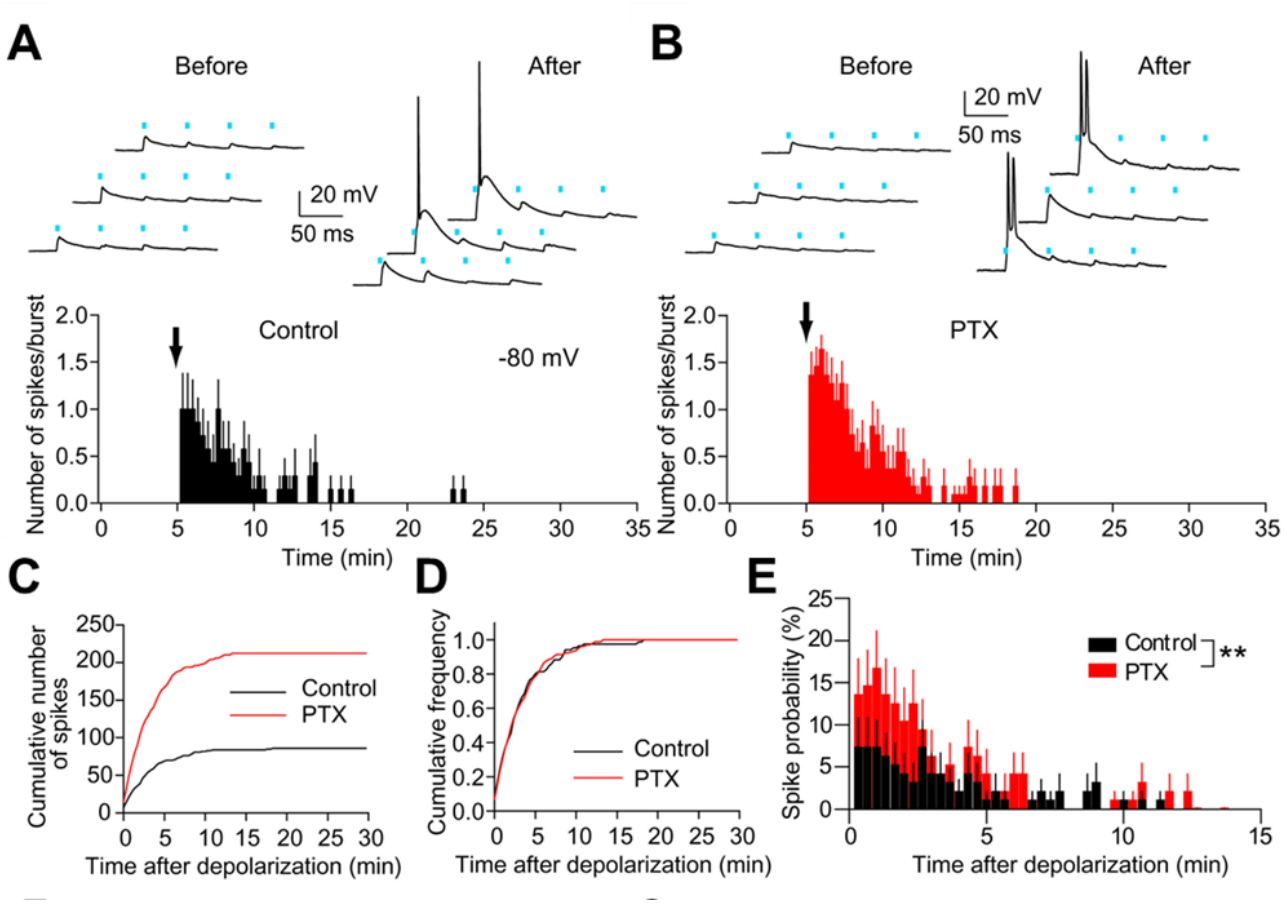

Figure 16. SuM inputs trigger spike generation in GCs by increasing excitatory drive associated with the induction of depol-eLTP

(A and B, Upper) Representative traces showing GC firing elicited by burst light illumination (four pulses, 20 Hz) before and after induction of depol-eLTP in the control (A) and in the presence of 100 μM picrotoxin (PTX) (B). (Lower) Time-course plots of the number of spikes per burst (control, n = 7; PTX, n = 11). After 5-min baseline (no spike), the recording was switched to voltage-clamp mode, and GCs were depolarized repetitively to induce depol-eLTP (arrow). Membrane potential was held at −80 mV to −85 mV in current-clamp mode. (C and D) Cumulative number of spikes (C) and frequency (D) in control and PTX (P = 0.054, Kolmogorov–Smirnov test). (E) Time-course plot of the spike probability after induction of depol-eLTP in control (n = 24) and PTX (n = 25). In the presence of PTX, induction of depol-eLTP significantly increased spike probability (P < 0.01, two-way ANOVA). Nonspiking cells were included in the analysis. Data are presented as mean ± SEM; **P < 0.01, ***P < 0.001.

I further examined SuM input-evoked GC firing at a more depolarized membrane potential (between −60 to −65 mV, referred to as −60 mV) in which GABAergic action is hyperpolarizing. Similar to the more negative membrane potential (−80 mV), I found that burst stimulation evoked

APs after LTP induction (36 %, 9 of 25 cells, Fig. 17A). When inhibition was blocked, the number of spikes and spike probability were increased (54%, 13 of 24 cells, Fig. 17B, C, and D), and the spike generation lasted longer than control (Fig. 17E). Taken together, these results indicate that SuM inputs can drive GC output by induction of depol-eLTP, and GABAergic co-transmission contributes to the regulation of GC spike generation irrespective of the membrane potentials.

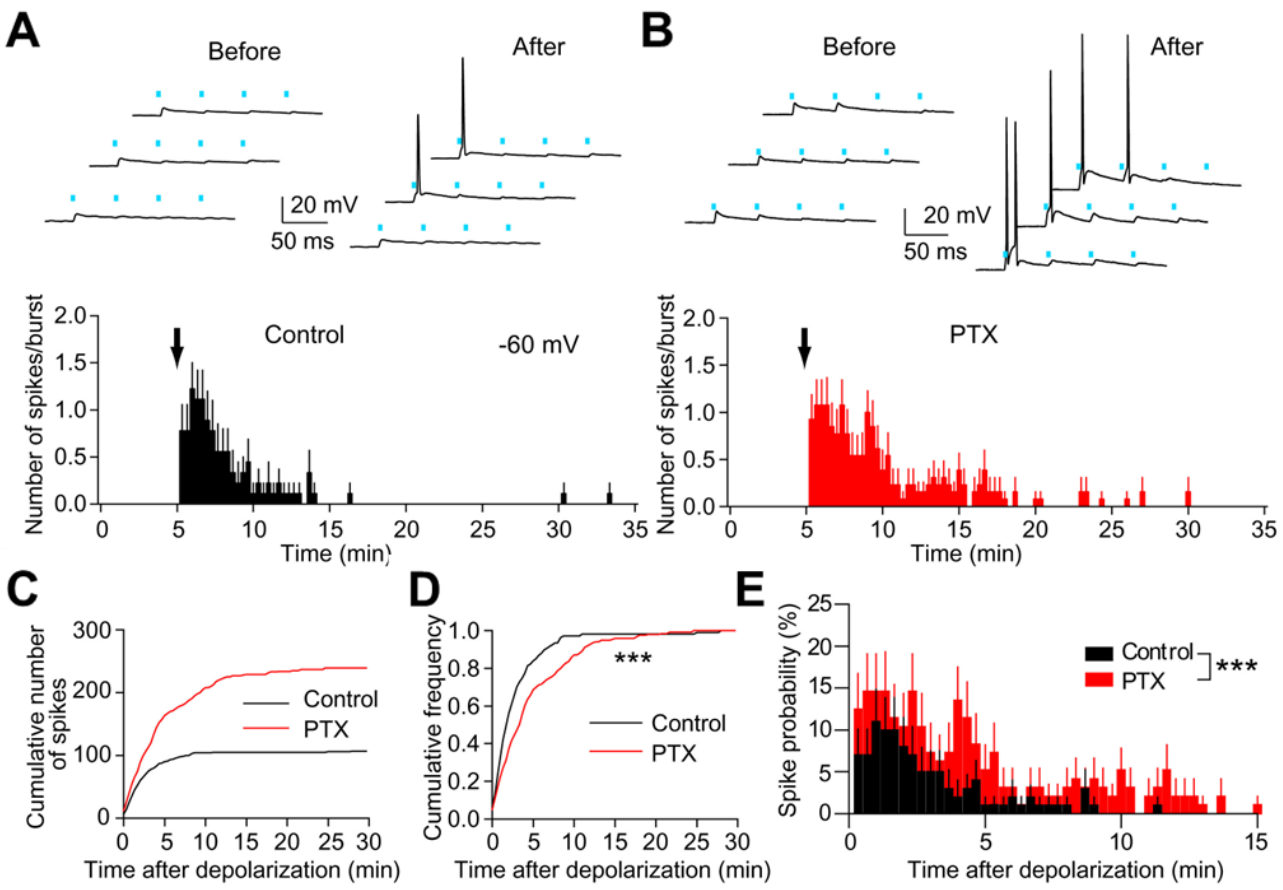

Figure 17. GABAergic co-transmission suppresses GC spike generation regardless of membrane potential

(A and B) Burst light illumination (four pulses, 20 Hz) was applied while GCs were held at −60 mV to −65 mV in current-clamp mode. Time-courses of the number of spikes per burst were plotted (control, n = 9; PTX, n = 13). (C and D) Cumulative number of spikes (C) and frequency (D) in control and PTX ($P < 0.001$, Kolmogorov−Smirnov test). (E) Time-course plot of the spike probability after induction of depol-eLTP in control (n = 25) and PTX (n = 24). In the presence of PTX, induction of depol-eLTP significantly increased spike probability ($P < 0.001$, two-way ANOVA). Nonspiking cells were included in the analysis. Data are presented as mean ± SEM; **$P < 0.01$, ***$P < 0.001$.

Chapter4. Discussion

In this study, I demonstrate that GC depolarization induces LTP of SuM-GC glutamatergic, but not GABAergic, co-transmission. This depol-eLTP requires postsynaptic Ca^{2+} elevation through L-VDCCs, postsynaptic CaMKII activity, and exocytosis of AMPARs and is expressed postsynaptically. I further found that excitatory SuM-GC synapses were likely toinclude silent synapses, and the LTP induction protocol triggered synapse unsilencing. Interestingly, depol-eLTP is exclusively induced at SuM-GC synapses but not at MPP-GC, IN-GC, SuM-IN or SuM-CA2 pyramidal neuron synapses. Depol-eLTP was heterosynaptically induced by MPP-driven GC firing, suggesting non-Hebbian form of plasticity. I finally reveal that selective LTP of glutamatergic co-transmission at SuM-GC synapses changes the E/I balance, makes excitatory effects dominate and consequently potentiates GC firiing. Our study shows that the balance of glutamatergic/GABAergic co-transmission is modulated in an activity-dependent manner. Depol-eLTP at SuM-GC synapses may contribute to network activity in the DG and SuM-DG pathway-dependent neural functions.

4.1 Activity-dependent change in the balance of glutamatergic and GABAergic co-transmission at SuM-GC synapses

Previous studies have reported that the balance of glutamate/GABA co-release in the lateral habenula was altered by depression and addiction (S. J. Shabel et al., 2014; F. J. Meye et al., 2016). In these neurological disorders, GABAergic co-transmission was reduced due to decreased

expression of GAD or VGAT. In contrast to these chronic presynaptic alterations, depol-eLTP of SuM-GC synapses is more rapidly expressed via postsynaptic modifications in response to physiological neural activity. Through this alteration of glutamatergic/GABAergic co-transmission ratio, depol-eLTP can achieve dynamic modulation of GC activity.

To induce depol-eLTP, I delivered repetitive depolarizing pulses to GCs. To mimic more physiological situations, I further showed that GC burst firing or TBS of the MPP inputs can trigger LTP at excitatory SuM-GC synapses. It is known that GC activity *in vivo* is sparse (T. Hainmueller & M. Bartos, 2020). At first glance, this evidence may appear to make it unlikely that depol-eLTP is induced by the natural activity patterns of GCs. However, some GCs are more active and often fire in burst patterns (M. Diamantaki st al., 2016; A. J. Pernía-Andrade & P. Jonas, 2014; D. Vandael et al., 2020; X. Zhang et al., 2020). Therefore, GC activity in behaving animals may trigger Ca^{2+} increases strong enough to induce depol-eLTP. Particularly, “superbursts” activity in GCs observed during mouse spatial navigation (D. Vandael et al., 2020) may be suitable for the induction of depol-eLTP.

The balance between excitation and inhibition is essential for computation in the neuronal circuits, and feedback and feedforward inhibition generally control excitatory transmission (J. S. Isaacson & M. Scanziani, 2013). However, such di-synaptic inhibition usually has some delay, allowing excitatory transmission before inhibition. A unique property of glutamate/GABA co-release is that both neurotransmitters are released from the individual presynaptic terminals (D. H.

Root et al., 2018), achieving very local and synchronous (without a monosynaptic delay mediated by feedforward inhibition) GABAergic inhibition. When the membrane potential of GCs was held at negative potential relative to E_{GABA}, blockade of GABAergic inhibition increased SuM input-evoked spike probability, indicating that GABAergic co-transmission serves as inhibition despite the depolarizing action of GABA at resting potential. This shunting inhibition seems prominent in glutamate/GABA co-release synapses, as both neurotransmitters are synchronously released from the same terminals, providing spatially and temporally matched inhibition to excitatory co-transmission. This more targeted form of inhibition (C. Q. Chiu et al., 2013) than the typical disynaptic feedforward inhibition, which could be spatially isolated from excitatory inputs, may exclude the possibility that the action of GABAergic co-transmission of SuM inputs is depolarizing (P. H. Chiang et al., 2012; A. T. Gulledge & G. J. Stuart, 2003). However, it should be noted that SuM neurons also excite dentate INs, driving feedforward inhibition to GCs (Y. Hashimotodani et al., 2018; M. I. Ajibola et al., 2021). Therefore, I cannot exclude the possibility that GABAergic inputs derived from feedforward inhibition recruited by SuM inputs contribute to regulation of GC firing.

I found that silent synapses might exist at SuM-GC synapses, and the depol-eLTP induction protocol induced synapse unsilencing. In this study, I recorded from GCs with a low input resistance (< 300 MΩ), which are regarded as mature GCs (C. Schmidt-Hieber et al., 2004). Given that silent synapses are generally observed in the young brain (G. A. Kerchner & R. A.

Nicoll, 2008), our results suggest that mature GCs contain exceptionally abundant silent synapses at SuM-GC synapses. The sparse activity of GCs could account for our observations. If some GCs have never fired in bursts (silent GCs), such cells would not experience depol-eLTP, preventing NMDAR-only synapses from adding new AMPARs. It has been reported that dendritic complexity and the intrinsic excitability of GCs are correlated with GC activity (M. Diamantaki et al., 2016; X. Zhang et al., 2020). Accordingly, silent GCs with less branched dendrites and low intrinsic excitability may account for a large fraction of NMDAR-only synapses at SuM-GC synapses. Future studies will have to investigate the relationship between dendritic morphology and proportion of silent synapses.

4.2 Mechanism of depol-eLTP

Depol-eLTP is similar to the early studies showing that CA3-CA1 synapses elicit L-VDCC-dependent, but NMDAR-independent form of LTP (L. Aniksztejn & Y. Ben-Ari, 1991; L. M. Grover & T. J. Teyler, 1990; Y. Y. Huang & R. C. Malenka,1993). A follow-up study demonstrated that L-VDCC-dependent form of LTP induced by postsynaptic depolarization in the CA1 pyramidal neurons requires CaMKII and shares the same expression mechanisms with NMDAR-dependent LTP at CA3-CA1 synapses (H. K. Kato et al., 2009). NMDAR-dependent CA1 LTP is the most studied and best known form of plasticity, thereby regarding this LTP as the primary model for understanding LTP. A widely accepted model of CA1 LTP (B. E. Herring & R. A. Nicoll, 2016; J.

Lisman et al., 2012; D. Choquet, 2018; B. G. Hiester et al., 2018) indicates that two parallel pathways occur during the induction of LTP: trapping of surface diffusing AMPARs at the synapses and exocytosis of AMPAR-containing vesicles. Ca^{2+} entry through NMDARs initiates these processes, and once AMPARs move in the synapses, CaMKII and downstream signaling cascades contribute to the stabilization of receptors in the PSD (postsynaptic density) where receptors are clustered. Given that depol-eLTP requires postsynaptic CaMKII activity and exocytosis of AMPARs, it seems likely that the postsynaptic Ca^{2+} increases through L-VDCCs rather than NMDARs trigger synaptic insertion of AMPARs via exocytosis of AMPARs and activation of CaMKII. The critical question is how L-VDCCs substitute for NMDARs. Generally, the localized Ca^{2+} elevation through NMDARs in the spine drives localized activation of CaMKII in the same spine to induce LTP (J. Lisman et al, 2012). Given that L-VDCCs trigger non-localized, bulk Ca^{2+} increases, how does this Ca^{2+} increase activate CaMKII? Interestingly, SuM terminals make heterogeneous forms of synaptic contacts to GCs by forming symmetric and asymmetric synapses on the soma, dendritic shafts, and spines (F. Billwiller et al., 2020; J. L. Boulland et al., 2009; J. A. Dent et al., 1983; R. Soussi et al., 2010). Because increases in the Ca^{2+} concentrations following depolarization are obviously different among the soma, dendritic shafts, and spines, it is likely that CaMKII activation is differently regulated by different Ca^{2+} levels in various subcellular compartments. For example, if L-VDCCs are localized close to the PSDs at the soma or dendritic shafts of SuM-GC glutamatergic synapses, local Ca^{2+} levels could be high enough to sufficiently

activate CaMKII to induce depo-eLTP. To reveal this, the distribution of L-VDCCs in SuM-GC synapses and the compartments of synapses that undergo depol-eLTP have to be known in future studies.

Depol-eLTP shows large transient potentiation immediately after postsynaptic depolarization, which was less affected by CaMKII inhibitors and inhibition of exocytosis. Similar results were found in NMDAR-dependent CA1 LTP, demonstrating that inhibition of exocytosis does not affect early phase of LTP (P. M. Lledo et al., 1998; B. G. Hiester et al., 2018; A. C. Penn et al., 2017, D. Wu et al., 2017). The early phase of potentiation is attributed to the capture of pre-existing surface diffusing AMPARs J. Lisman et al., 2012; B. G. Hiester et al., 2018; A. C. Penn et al., 2017; A. J. Granger et al., 2013). Interestingly, I found that inhibition of glutamate uptake by DL-threo-β-benzyloxyaspartic acid (TBOA) increased SuM-GC oEPSCs, but not MPP-EPSCs (data not shown). In many synapses, inhibition of glutamate uptake influences the kinetics of AMPAR-EPSCs only when AMPAR desensitization is blocked (A. V. Tzingounis & J. I. Wadiche, 2007). Therefore, TBOA-induced increase in SuM-GC oEPSCs with AMPAR desensitization intact suggests that excitatory SuM-GC synapses may have exceptionally a large extrasynaptic pool of surface AMPARs (A. J. Granger et al., 2013). Further investigation will be required to examine whether these extrasynaptic AMPARs can contribute to the initiation of the early phase of potentiation by transient trapping in the PSD by Ca^{2+} influx. However, I cannot exclude the possibility that post-translational modifications of AMPARs, such as increase in conductance and

open probability, following depolarization-induced Ca^{2+} elevation may also contribute to the early phase of potentiation.

Although somatic depolarization of GCs induces large Ca^{2+} elevation in both proximal and distal dendrites (G. Stocca et al., 2008), depol-eLTP is observed exclusively at SuM inputs, but not at MPP inputs. Furthermore, SuM inputs elicit depol-eLTP specifically targeting GCs, but not INs and CA2 pyramidal neurons. What molecular mechanisms determine the synapse type- and target-specificity of LTP? There are several explanations for this. First, an unknown molecular sensor for Ca^{2+} ions may be specifically expressed in SuM-GC synapses and contribute to the increase in the number of synaptic AMPARs. Second, as prominent characteristics of excitatory SuM-GC synapses, I have shown a high NMDAR/AMPAR ratio and the existence of silent synapses. These findings imply that excitatory SuM-GC synapses may have many slots for trapping AMPARs (AMPAR-silent module) in the PSD (J. Lisman & S. Raghavachari, 2006). Finally, the location of synapses relative to the soma may be critical for induction of LTP. Considering that backpropagating AP-induced Ca^{2+} transients show a distance-dependent attenuation in the GCs (R. Krueppel et al., 2011) but see (G. Stocca et al., 2008), a rise in the intracellular Ca^{2+} is higher in the SuM inputs at the soma or close to the soma, thereby reducing the threshold for the induction of depol-eLTP. Future studies may be needed to investigate all these possibilities.

4.3 Physiological relevance of depol-eLTP in the DG network

Hashimotodani et al. (2018) previously reported that SuM inputs have net excitatory effects on GCs and contribute to the facilitation of GC firing when associated with PP inputs (Y. Hashimotodani et al., 2018). Our present study extends this previous study. Once depol-eLTP is induced, SuM inputs exert strong excitatory effects on GCs and elicit APs, especially within 10 min after LTP induction. After this period, SuM inputs failed to trigger spikes. This time window corresponds to the magnitude of oEPSC potentiation, showing huge potentiation followed by a stable potentiation phase. In the stable phase, potentiated SuM inputs associated with PP inputs can excite GCs more efficiently than under basal conditions. This suggests that depol-eLTP primes the SuM-GC synapses for GC firing. Thus, by establishing a new glutamatergic/GABAergic co-transmission ratio, solo SuM inputs or the association of SuM and PP inputs can trigger enhancement of AP generation in GCs. A large population of SuM neurons is known to discharge rhythmically with a theta rhythm (I. J. Kirk & N. McNaughton, 1991; B. Kocsis & R. P. Vertes, 1994). Therefore, once depol-eLTP is heterosynaptically induced by entorhinal cortical inputs, it is likely that potentiated SuM inputs can frequently discharge GCs. The consequences of the GC output on its target are frequency dependent. High-frequency GC firing drives CA3 pyramidal neuron discharge, whereas low-frequency GC firing drives CA3 IN discharge (D. A. Henze et al., 2002). This GC firing frequency-dependent outcome in the CA3 pyramidal neurons suggests that depol-eLTP may dramatically increase CA3 output through the enhancement of GC firing and

consequently the DG-CA3-CA1 trisynaptic circuit. Interestingly, a recent study reported that glutamatergic co-transmission at SuM-GC synapses is required for spatial memory retrieval (Y. Li et al., 2020). Given that memory engram GCs show LTP-like synaptic properties (T. J. Ryan et al., 2015), depol-eLTP at SuM-GC synapses may be induced during memory formation, and after memory encoding and consolidation, depol-eLTP in engram GCs may contribute to memory retrieval through the potentiated SuM-DG excitatory pathway.

In addition to the SuM, GCs also receive local excitatory inputs from hilar mossy cells, which modulate GC activity through direct excitation and IN-mediated feed-forward inhibition (H. E. Scharfman, 2016). It has been reported that presynaptic LTP is selectively expressed at mossy cell inputs onto GCs, but not at mossy cell inputs onto INs and facilitates GC output by increasing excitation/inhibition balance (Y. Hashimotodani et al., 2017). Together with the present study, the results indicate that the DG network is dynamically regulated by mossy cell-mediated local and SuM-mediated subcortical pathways through two different forms of LTP.

4.4 Outlook

The present study reveals that co-release of glutamate and GABA, surprising feature of SuM-GC synapses, has functional meanings. Namely, the balance between excitation and inhibition can be dynamically modulated in a non-Hebbian manner. Depending of the inputs from enthorinal cortex, the excitatory inputs from SuM can be modulated. SuM is recently recognized as an

important center for cognition and emotion (Chen et al., 2020; Kesner et al., 2023). In addition, SuM synchronizes spike-time coordination in the prefrontal-thalamo-hippocampal circuit during navigation (Ito et al., 2018). Given the importance of SuM described above, further characterization of neurocircuits underlying the signal transfer from SuM to hippocampus is important for systems neuroscience of cognitive process.

For the cellular level, co-release of glutamate and GABA is very unique, given that classically only one type of neurotransmitter is released from a single terminal. Recently, Kim et al. (2022) have shown that two opposing transmitters, glutamate and GABA can be packed in the same synaptic vesicles. However, it is unknown if the same mechanism applies to SuM-GC synapses. This issue must be resolved not only by electrophysiology, but also by more direct methods such as super-resolution imaging and electron microscopy in the future studies.

Chapter5. References

Ajibola MI, Wu JW, Abdulmajeed WI, Lien CC. Hypothalamic Glutamate/GABA Cotransmission Modulates Hippocampal Circuits and Supports Long-Term Potentiation. J Neurosci. 2021 41(39):8181-8196. doi: 10.1523/JNEUROSCI.0410-21.2021. Epub 2021 Aug 11. PMID: 34380766; PMCID: PMC8482861.

Amaral DG, Scharfman HE, Lavenex P. The dentate gyrus: fundamental neuroanatomical organization (dentate gyrus for dummies). Prog Brain Res. 2007 163:3-22. doi: 10.1016/S0079-6123(07)63001-5. PMID: 17765709; PMCID: PMC2492885.

Aniksztejn L, Ben-Ari Y. Novel form of long-term potentiation produced by a K^+ channel blocker in the hippocampus. Nature. 1991 349(6304):67-9. doi: 10.1038/349067a0. PMID: 1845914.

Billwiller F, Castillo L, Elseedy H, Ivanov AI, Scapula J, Ghestem A, Carponcy J, Libourel PA, Bras H, Abdelmeguid NE, Krook-Magnuson E, Soltesz I, Bernard C, Luppi PH, Esclapez M. GABA-glutamate supramammillary neurons control theta and gamma oscillations in the dentate gyrus during paradoxical (REM) sleep. Brain Struct Funct. 2020 225(9):2643-2668. doi: 10.1007/s00429-020-02146-y. PMID: 32970253; PMCID: PMC7674372.

Boulland JL, Jenstad M, Boekel AJ, Wouterlood FG, Edwards RH, Storm-Mathisen J, Chaudhry FA. Vesicular glutamate and GABA transporters sort to distinct sets of vesicles in a population of presynaptic terminals. Cereb Cortex. 2009 19(1):241-8. doi: 10.1093/cercor/bhn077. Epub 2008 May 22. PMID: 18502731; PMCID: PMC3202896.

Bragin A, Jandó G, Nádasdy Z, Hetke J, Wise K, Buzsáki G. Gamma (40-100 Hz) oscillation in the hippocampus of the behaving rat. J Neurosci. 1995 15(1 Pt 1):47-60. doi: 10.1523/JNEUROSCI.15-01-00047.1995. PMID: 7823151; PMCID: PMC6578273.

Caillard O, Ben-Ari Y, Gaiarsa JL. Long-term potentiation of GABAergic synaptic transmission in neonatal rat hippocampus. J Physiol. 1999 518(Pt 1):109-19. doi: 10.1111/j.1469-7793.1999.0109r.x. PMID: 10373693; PMCID: PMC2269393.

Chen S, He L, Huang AJY, Boehringer R, Robert V, Wintzer ME, Polygalov D, Weitemier AZ, Tao Y, Gu M, Middleton SJ, Namiki K, Hama H, Therreau L, Chevaleyre V, Hioki H, Miyawaki A, Piskorowski RA, McHugh TJ. A hypothalamic novelty signal modulates hippocampal memory. Nature. 2020 586(7828):270-274. doi: 10.1038/s41586-020-2771-1. PMID: 32999460.

Chiang PH, Wu PY, Kuo TW, Liu YC, Chan CF, Chien TC, Cheng JK, Huang YY, Chiu CD, Lien CC. GABA is depolarizing in hippocampal dentate granule cells of the adolescent and adult rats. J Neurosci. 2012 32(1):62-7. doi: 10.1523/JNEUROSCI.3393-11.2012. PMID: 22219270; PMCID: PMC6621339.

Chiu CQ, Lur G, Morse TM, Carnevale NT, Ellis-Davies GC, Higley MJ. Compartmentalization of GABAergic inhibition by dendritic spines. Science. 2013 340(6133):759-62. doi: 10.1126/science.1234274. PMID: 23661763; PMCID: PMC3752161.

Choquet D. Linking Nanoscale Dynamics of AMPA Receptor Organization to Plasticity of Excitatory Synapses and Learning. J Neurosci. 2018 38(44):9318-9329. doi: 10.1523/JNEUROSCI.2119-18.2018. PMID: 30381423; PMCID: PMC6705996.

Dent JA, Galvin NJ, Stanfield BB, Cowan WM. The mode of termination of the hypothalamic projection to the dentate gyrus: an EM autoradiographic study. Brain Res. 1983 258(1):1-10. doi: 10.1016/0006-8993(83)91220-9. PMID: 24010158.

Diamantaki M, Frey M, Berens P, Preston-Ferrer P, Burgalossi A. Sparse activity of identified dentate granule cells during spatial exploration. Elife. 2016 5:e20252. doi: 10.7554/eLife.20252. PMID: 27692065; PMCID: PMC5077296.

Fasano C, Rocchetti J, Pietrajtis K, Zander JF, Manseau F, Sakae DY, Marcus-Sells M, Ramet L, Morel LJ, Carrel D, Dumas S, Bolte S, Bernard V, Vigneault E, Goutagny R, Ahnert-Hilger G, Giros B, Daumas S, Williams S, El Mestikawy S. Regulation of the Hippocampal Network by VGLUT3-Positive CCK- GABAergic Basket Cells. Front Cell Neurosci. 2017 11:140. doi: 10.3389/fncel.2017.00140. PMID: 28559797; PMCID: PMC5432579.

Ge S, Yang CH, Hsu KS, Ming GL, Song H. A critical period for enhanced synaptic plasticity in newly generated neurons of the adult brain. Neuron. 2007 54(4):559-66. doi: 10.1016/j.neuron.2007.05.002. PMID: 17521569; PMCID: PMC2040308.

Goode TD, Tanaka KZ, Sahay A, McHugh TJ. An Integrated Index: Engrams, Place Cells, and Hippocampal Memory. Neuron. 2020 107(5):805-820. doi: 10.1016/j.neuron.2020.07.011. PMID: 32763146; PMCID: PMC7486247.

Granger AJ, Shi Y, Lu W, Cerpas M, Nicoll RA. LTP requires a reserve pool of glutamate receptors independent of subunit type. Nature. 2013 493(7433):495-500. doi: 10.1038/nature11775. PMID: 23235828; PMCID: PMC3998843.

Grover LM, Teyler TJ. Two components of long-term potentiation induced by different patterns of afferent activation. Nature. 1990 347(6292):477-9. doi: 10.1038/347477a0. PMID: 1977084.
Gulledge AT, Stuart GJ. Excitatory actions of GABA in the cortex. Neuron. 2003 37(2):299-309. doi: 10.1016/s0896-6273(02)01146-7. PMID: 12546824.

Haglund L, Swanson LW, Köhler C. The projection of the supramammillary nucleus to the hippocampal formation: an immunohistochemical and anterograde transport study with the lectin PHA-L in the rat. J Comp Neurol. 1984 229(2):171-85. doi: 10.1002/cne.902290204. PMID: 6501599.

Hainmueller T, Bartos M. Dentate gyrus circuits for encoding, retrieval and discrimination of episodic memories. Nat Rev Neurosci. 2020 21(3):153-168. doi: 10.1038/s41583-019-0260-z. Epub 2020 Feb 10. PMID: 32042144; PMCID: PMC7115869.

Hashimotodani Y, Karube F, Yanagawa Y, Fujiyama F, Kano M. Supramammillary Nucleus Afferents to the Dentate Gyrus Co-release Glutamate and GABA and Potentiate Granule Cell Output. Cell Rep. 2018 25(10):2704-2715.e4. doi: 10.1016/j.celrep.2018.11.016. PMID: 30517859.

Hashimotodani Y, Nasrallah K, Jensen KR, Chávez AE, Carrera D, Castillo PE. LTP at Hilar Mossy Cell-Dentate Granule Cell Synapses Modulates Dentate Gyrus Output by Increasing Excitation/Inhibition Balance. Neuron. 2017 95(4):928-943.e3. doi: 10.1016/j.neuron.2017.07.028. PMID: 28817805; PMCID: PMC5609819.

Henze DA, Wittner L, Buzsáki G. Single granule cells reliably discharge targets in the hippocampal CA3 network in vivo. Nat Neurosci. 2002 5(8):790-5. doi: 10.1038/nn887. PMID: 12118256.

Herring BE, Nicoll RA. Long-Term Potentiation: From CaMKII to AMPA Receptor Trafficking. Annu Rev Physiol. 2016 78:351-65. doi: 10.1146/annurev-physiol-021014-071753. PMID: 26863325.

Hiester BG, Becker MI, Bowen AB, Schwartz SL, Kennedy MJ. Mechanisms and Role of Dendritic Membrane Trafficking for Long-Term Potentiation. Front Cell Neurosci. 2018 12:391. doi: 10.3389/fncel.2018.00391. PMID: 30425622; PMCID: PMC6218485.

Huang YY, Malenka RC. Examination of TEA-induced synaptic enhancement in area CA1 of the hippocampus: the role of voltage-dependent Ca^{2+} channels in the induction of LTP. J Neurosci. 1993 13(2):568-76. doi: 10.1523/JNEUROSCI.13-02-00568.1993. PMID: 8381168; PMCID: PMC6576643.

Ito HT, Moser EI, Moser MB. Supramammillary Nucleus Modulates Spike-Time Coordination in the Prefrontal-Thalamo-Hippocampal Circuit during Navigation. Neuron. 2018 99(3):576-587.e5. doi: 10.1016/j.neuron.2018.07.021. PMID: 30092214.

Kano M, Rexhausen U, Dreessen J, Konnerth A. Synaptic excitation produces a long-lasting rebound potentiation of inhibitory synaptic signals in cerebellar Purkinje cells. Nature. 1992 356(6370):601-4. doi: 10.1038/356601a0. PMID: 1313949.

Kato HK, Watabe AM, Manabe T. Non-Hebbian synaptic plasticity induced by repetitive postsynaptic action potentials. J Neurosci. 2009 29(36):11153-60. doi: 10.1523/JNEUROSCI.5881-08.2009. PMID: 19741122; PMCID: PMC6665946.

Kerchner GA, Nicoll RA. Silent synapses and the emergence of a postsynaptic mechanism for LTP. Nat Rev Neurosci. 2008 9(11):813-25. doi: 10.1038/nrn2501. Erratum in: Nat Rev Neurosci. 2009 10(3):242. PMID: 18854855; PMCID: PMC2819160.

Kesner AJ, Mozaffarilegha M, Thirtamara Rajamani K, Arima Y, Harony-Nicolas H, Hashimotodani Y, Ito HT, Song J, Ikemoto S. Hypothalamic Supramammillary Control of Cognition and Motivation. J Neurosci. 2023 43(45):7538-7546. doi: 10.1523/JNEUROSCI.1320-23.2023. PMID: 37940587; PMCID: PMC10634554.

Kim S, Wallace ML, El-Rifai M, Knudsen AR, Sabatini BL. Co-packaging of opposing neurotransmitters in individual synaptic vesicles in the central nervous system. Neuron. 2022 110(8):1371-1384.e7. doi: 10.1016/j.neuron.2022.01.007. PMID: 35120627; PMCID: PMC9056948.

Kirk IJ, McNaughton N. Supramammillary cell firing and hippocampal rhythmical slow activity. Neuroreport. 1991 2(11):723-5. doi: 10.1097/00001756-199111000-00023. PMID: 1810464.

Knierim JJ, Neunuebel JP. Tracking the flow of hippocampal computation: Pattern separation, pattern completion, and attractor dynamics. Neurobiol Learn Mem. 2016 129:38-49. doi: 10.1016/j.nlm.2015.10.008. Epub 2015 Oct 26. PMID: 26514299; PMCID: PMC4792674.

Kocsis B, Vertes RP. Characterization of neurons of the supramammillary nucleus and mammillary body that discharge rhythmically with the hippocampal theta rhythm in the rat. J Neurosci. 1994 14(11 Pt 2):7040-52. doi: 10.1523/JNEUROSCI.14-11-07040.1994. PMID: 7965097; PMCID: PMC6577300.

Kohara K, Pignatelli M, Rivest AJ, Jung HY, Kitamura T, Suh J, Frank D, Kajikawa K, Mise N, Obata Y, Wickersham IR, Tonegawa S. Cell type-specific genetic and optogenetic tools reveal hippocampal CA2 circuits. Nat Neurosci. 2014 17(2):269-79. doi: 10.1038/nn.3614. PMID: 24336151; PMCID: PMC4004172.

Krueppel R, Remy S, Beck H. Dendritic integration in hippocampal dentate granule cells. Neuron. 2011 71(3):512-28. doi: 10.1016/j.neuron.2011.05.043. PMID: 21835347.

Kurotani T, Yamada K, Yoshimura Y, Crair MC, Komatsu Y. State-dependent bidirectional modification of somatic inhibition in neocortical pyramidal cells. Neuron. 2008 57(6):905-16. doi: 10.1016/j.neuron.2008.01.030. PMID: 18367091; PMCID: PMC2880402.

Li Y, Bao H, Luo Y, Yoan C, Sullivan HA, Quintanilla L, Wickersham I, Lazarus M, Shih YI, Song J. Supramammillary nucleus synchronizes with dentate gyrus to regulate spatial memory retrieval through glutamate release. Elife. 2020 9:e53129. doi: 10.7554/eLife.53129. PMID: 32167473; PMCID: PMC7069722.

Lisman J, Raghavachari S. A unified model of the presynaptic and postsynaptic changes during LTP at CA1 synapses. Sci STKE. 2006 2006(356):re11. doi: 10.1126/stke.3562006re11. PMID: 17033044.

Lisman J, Yasuda R, Raghavachari S. Mechanisms of CaMKII action in long-term potentiation. Nat Rev Neurosci. 2012 13(3):169-82. doi: 10.1038/nrn3192. PMID: 22334212; PMCID: PMC4050655.

Lledo PM, Zhang X, Südhof TC, Malenka RC, Nicoll RA. Postsynaptic membrane fusion and long-term potentiation. Science. 1998 279(5349):399-403. doi: 10.1126/science.279.5349.399. PMID: 9430593.

Lourenço J, Pacioni S, Rebola N, van Woerden GM, Marinelli S, DiGregorio D, Bacci A. Non-associative potentiation of perisomatic inhibition alters the temporal coding of neocortical layer 5 pyramidal neurons. PLoS Biol. 2014 12(7):e1001903. doi: 10.1371/journal.pbio.1001903. PMID: 25003184; PMCID: PMC4086817.

Malenka RC, Nicoll RA. Long-term potentiation--a decade of progress? Science. 1999 285(5435):1870-4. doi: 10.1126/science.285.5435.1870. PMID: 10489359.

Malinow R, Schulman H, Tsien RW. Inhibition of Postsynaptic PKC or CaMKII Blocks Induction But Not Expression of LTP. Science. 1989 245,862-866. DOI:10.1126/science.2549638

Meye FJ, Soiza-Reilly M, Smit T, Diana MA, Schwarz MK, Mameli M. Shifted pallidal co-release of GABA and glutamate in habenula drives cocaine withdrawal and relapse. Nat Neurosci. 2016 19(8):1019-24. doi: 10.1038/nn.4334. Erratum in: Nat Neurosci. 2020 23(4):594. PMID: 27348214.

Nguyen PV, Woo NH. Regulation of hippocampal synaptic plasticity by cyclic AMP-dependent protein kinases. Prog Neurobiol. 2003 71(6):401-37. doi: 10.1016/j.pneurobio.2003.12.003. PMID: 15013227.

Pan WX, McNaughton N. The supramammillary area: its organization, functions and relationship to the hippocampus. Prog Neurobiol. 2004 74(3):127-66. doi: 10.1016/j.pneurobio.2004.09.003. PMID: 15556285.

Pavlides C, Greenstein YJ, Grudman M, Winson J. Long-term potentiation in the dentate gyrus is induced preferentially on the positive phase of theta-rhythm. Brain Res. 1988 439(1-2):383-7. doi: 10.1016/0006-8993(88)91499-0. PMID: 3359196.

Pedersen NP, Ferrari L, Venner A, Wang JL, Abbott SBG, Vujovic N, Arrigoni E, Saper CB, Fuller PM. Supramammillary glutamate neurons are a key node of the arousal system. Nat Commun. 2017 8(1):1405. doi: 10.1038/s41467-017-01004-6. PMID: 29123082; PMCID: PMC5680228.

Pelkey KA, Calvigioni D, Fang C, Vargish G, Ekins T, Auville K, Wester JC, Lai M, Mackenzie-Gray Scott C, Yuan X, Hunt S, Abebe D, Xu Q, Dimidschstein J, Fishell G, Chittajallu R, McBain CJ. Paradoxical network excitation by glutamate release from VGluT3^{+} GABAergic interneurons. Elife. 2020 9:e51996. doi: 10.7554/eLife.51996. PMID: 32053107; PMCID: PMC7039679.

Penn AC, Zhang CL, Georges F, Royer L, Breillat C, Hosy E, Petersen JD, Humeau Y, Choquet D. Hippocampal LTP and contextual learning require surface diffusion of AMPA receptors. Nature. 2017 549(7672):384-388. doi: 10.1038/nature23658. PMID: 28902836; PMCID: PMC5683353.

Pernía-Andrade AJ, Jonas P. Theta-gamma-modulated synaptic currents in hippocampal granule cells in vivo define a mechanism for network oscillations. Neuron. 2014 81(1):140-52. doi: 10.1016/j.neuron.2013.09.046. Epub 2013 Dec 12. PMID: 24333053; PMCID: PMC3909463.

Renouard L, Billwiller F, Ogawa K, Clément O, Camargo N, Abdelkarim M, Gay N, Scoté-Blachon C, Touré R, Libourel PA, Ravassard P, Salvert D, Peyron C, Claustrat B, Léger L, Salin P, Malleret G, Fort P, Luppi PH. The supramammillary nucleus and the claustrum activate the cortex during REM sleep. Sci Adv. 2015 1(3):e1400177. doi: 10.1126/sciadv.1400177. PMID: 26601158; PMCID: PMC4640625.

Robert V, Therreau L, Chevaleyre V, Lepicard E, Viollet C, Cognet J, Huang AJ, Boehringer R, Polygalov D, McHugh TJ, Piskorowski RA. Local circuit allowing hypothalamic control of hippocampal area CA2 activity and consequences for CA1. Elife. 2021 10:e63352. doi: 10.7554/eLife.63352. PMID: 34003113; PMCID: PMC8154026.

Root DH, Mejias-Aponte CA, Zhang S, Wang HL, Hoffman AF, Lupica CR, Morales M. Single rodent mesohabenular axons release glutamate and GABA. Nat Neurosci. 2014 17(11):1543-51. doi: 10.1038/nn.3823. PMID: 25242304; PMCID: PMC4843828.

Root DH, Zhang S, Barker DJ, Miranda-Barrientos J, Liu B, Wang HL, Morales M. Selective Brain Distribution and Distinctive Synaptic Architecture of Dual Glutamatergic-GABAergic Neurons. Cell Rep. 2018 23(12):3465-3479. doi: 10.1016/j.celrep.2018.05.063. PMID: 29924991; PMCID: PMC7534802.

Ryan TJ, Roy DS, Pignatelli M, Arons A, Tonegawa S. Memory. Engram cells retain memory under retrograde amnesia. Science. 2015 348(6238):1007-13. doi: 10.1126/science.aaa5542. PMID: 26023136; PMCID: PMC5583719.

Sauer JF, Strüber M, Bartos M. Interneurons provide circuit-specific depolarization and hyperpolarization. J Neurosci. 2012 32(12):4224-9. doi: 10.1523/JNEUROSCI.5702-11.2012. PMID: 22442084; PMCID: PMC6621207.

Scharfman HE. The enigmatic mossy cell of the dentate gyrus. Nat Rev Neurosci. 2016 17(9):562-75. doi: 10.1038/nrn.2016.87. PMID: 27466143; PMCID: PMC5369357.

Schmidt-Hieber C, Jonas P, Bischofberger J. Enhanced synaptic plasticity in newly generated granule cells of the adult hippocampus. Nature. 2004 429(6988):184-7. doi: 10.1038/nature02553. PMID: 15107864.

Shabel SJ, Proulx CD, Piriz J, Malinow R. Mood regulation. GABA/glutamate co-release controls habenula output and is modified by antidepressant treatment. Science. 2014 345(6203):1494-8. doi: 10.1126/science.1250469. PMID: 25237099; PMCID: PMC4305433.

Sieber AR, Min R, Nevian T. Non-Hebbian long-term potentiation of inhibitory synapses in the thalamus. J Neurosci. 2013 33(40):15675-85. doi: 10.1523/JNEUROSCI.0247-13.2013. PMID: 24089475; PMCID: PMC6618469.

Skaggs WE, McNaughton BL, Wilson MA, Barnes CA. Theta phase precession in hippocampal neuronal populations and the compression of temporal sequences. Hippocampus. 1996 6(2):149-72. doi: 10.1002/(SICI)1098-1063(1996)6:2<149::AID-HIPO6>3.0.CO;2-K. PMID: 8797016.

Soussi R, Zhang N, Tahtakran S, Houser CR, Esclapez M. Heterogeneity of the supramammillary-hippocampal pathways: evidence for a unique GABAergic neurotransmitter phenotype and regional differences. Eur J Neurosci. 2010 32(5):771-85. doi: 10.1111/j.1460-9568.2010.07329.x. PMID: 20722723; PMCID: PMC2974797.

Staley KJ, Mody I. Shunting of excitatory input to dentate gyrus granule cells by a depolarizing GABAA receptor-mediated postsynaptic conductance. J Neurophysiol. 1992 68(1):197-212. doi: 10.1152/jn.1992.68.1.197. PMID: 1381418.

Stocca G, Schmidt-Hieber C, Bischofberger J. Differential dendritic Ca^{2+} signalling in young and mature hippocampal granule cells. J Physiol. 2008 586(16):3795-811. doi: 10.1113/jphysiol.2008.155739. PMID: 18591186; PMCID: PMC2538933.

Tritsch NX, Granger AJ, Sabatini BL. Mechanisms and functions of GABA co-release. Nat Rev Neurosci. 2016 17(3):139-45. doi: 10.1038/nrn.2015.21. PMID: 26865019; PMCID: PMC6980171.

Trudeau LE, El Mestikawy S. Glutamate Cotransmission in Cholinergic, GABAergic and Monoamine Systems: Contrasts and Commonalities. Front Neural Circuits. 2018 12:113. doi: 10.3389/fncir.2018.00113. PMID: 30618649; PMCID: PMC6305298.

Tzingounis AV, Wadiche JI. Glutamate transporters: confining runaway excitation by shaping synaptic transmission. Nat Rev Neurosci. 2007 8(12):935-47. doi: 10.1038/nrn2274. PMID: 17987031.

Uchida N. Bilingual neurons release glutamate and GABA. Nat Neurosci. 2014 17(11):1432-4. doi: 10.1038/nn.3840. PMID: 25349905.

Vandael D, Borges-Merjane C, Zhang X, Jonas P. Short-Term Plasticity at Hippocampal Mossy Fiber Synapses Is Induced by Natural Activity Patterns and Associated with Vesicle Pool Engram Formation. Neuron. 2020 107(3):509-521.e7. doi: 10.1016/j.neuron.2020.05.013. PMID: 32492366; PMCID: PMC7427323.

Vertes RP, Kocsis B. Brainstem-diencephalo-septohippocampal systems controlling the theta rhythm of the hippocampus. Neuroscience. 1997 81(4):893-926. doi: 10.1016/s0306-4522(97)00239-x. PMID: 9330355.

Vertes RP. PHA-L analysis of projections from the supramammillary nucleus in the rat. J Comp Neurol. 1992 326(4):595-622. doi: 10.1002/cne.903260408. PMID: 1484125.

Wallace ML, Saunders A, Huang KW, Philson AC, Goldman M, Macosko EZ, McCarroll SA, Sabatini BL. Genetically Distinct Parallel Pathways in the Entopeduncular Nucleus for Limbic and Sensorimotor Output of the Basal Ganglia. Neuron. 2017 94(1):138-152.e5. doi: 10.1016/j.neuron.2017.03.017. PMID: 28384468; PMCID: PMC5439268.

Wu D, Bacaj T, Morishita W, Goswami D, Arendt KL, Xu W, Chen L, Malenka RC, Südhof TC. Postsynaptic synaptotagmins mediate AMPA receptor exocytosis during LTP. Nature. 2017 544(7650):316-321. doi: 10.1038/nature21720. PMID: 28355182; PMCID: PMC5734942.

Yoo JH, Zell V, Gutierrez-Reed N, Wu J, Ressler R, Shenasa MA, Johnson AB, Fife KH, Faget L, Hnasko TS. Ventral tegmental area glutamate neurons co-release GABA and promote positive reinforcement. Nat Commun. 2016 7:13697. doi: 10.1038/ncomms13697. PMID: 27976722; PMCID: PMC5171775.

Zhang X, Schlögl A, Jonas P. Selective Routing of Spatial Information Flow from Input to Output in Hippocampal Granule Cells. Neuron. 2020 107(6):1212-1225.e7. doi: 10.1016/j.neuron.2020.07.006. PMID: 32763145; PMCID: PMC7523402.